and GAPDH) or 1.2% (Ago2) agarose gels and visualized under UV illumination after staining with ethidium bromide.

Western blotting. Anti-human Ago2 rabbit polyclonal antibody (Upstate, Lake Placid, NY), anti-actin rabbit polyclonal antibody (Sigma–Aldrich), anti-GAPDH mouse monoclonal antibody (GeneTex Inc., San Antonio, TX), peroxidase-conjugated anti-rabbit IgG polyclonal antibody (Santa Cruz Biotechnology, Santa Cruz, CA), and peroxidase-conjugated anti-mouse IgG polyclonal antibody (Santa Cruz Biotechnology) were purchased. The nucleotide sequences of siRNA for GAPDH (siGAPDH) with a 2-nucleotide overhang (underline) were 5′-CCAAAUAUGAUGACAUCAAGAAGGUAG-3′ (sense) and 5′-ACCUUCUUGAUGUCAUCAUAUUUGGAU-3′ (antisense). The sequences of siGAPDH correspond to the nucleotide region 791–815.

Cell extracts were prepared with lysis buffer composed of 10 mM Tris (pH 7.5), 0.1% SDS, 50 μg/ml aprotinin, 200 μM leupeptin, 2 mM PMSF, and 100 μM pepstatin A. Total protein concentration was measured by using a BCA Protein Assay Reagent Kit. The cell extract was subjected to 10 or 15% SDS–PAGE and transferred electrophoretically to a polyvi-

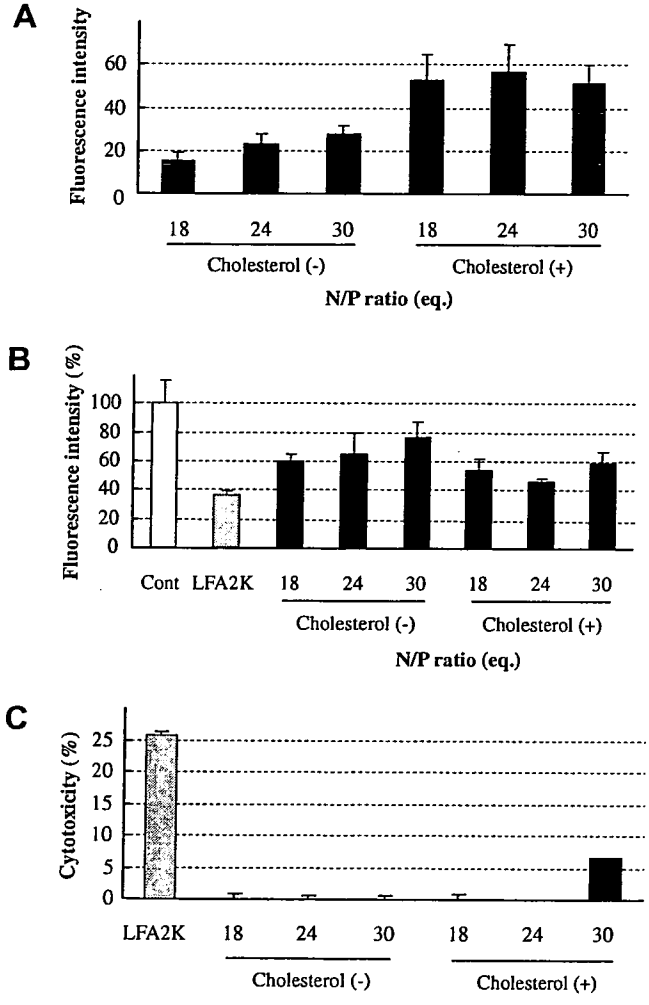

Fig. 1. Preparation of siRNA/PCLs complexes for siRNA transfection. (A) The amount of siRNA taken into HT1080 cells was determined after FAM-labeled siRNA/PCLs complexes had been allowed to interact with these cells for 4 h at 37 °C. PCLs with or without cholesterol were prepared and mixed with FAM-labeled siRNA at the various *N/P* ratios indicated in the figure. The fluorescence intensities of FAM in the cells were corrected for protein content. (B) RNAi efficiencies obtained by using PCLs were determined by conducting a quantitative gene silencing experiment. EGFP/HT-1080 cells were transfected with siEGFP complexed with PCLs (closed bar) or LFA2K (gray bar). The fluorescence intensity of EGFP was determined at 48 h post-transfection and corrected for protein content. The fluorescence intensity indicated as control (Cont, open bar) was that of cells not transfected with siRNA. Data represent the percent of control fluorescence intensity. (C) Cytotoxicity of PCLs against EGFP/HT1080 cells was determined. PCLs (closed bar) or LFA2K (gray bar) carrying siEGFP were allowed to interact with EGFP/HT1080 cells for 4 h at 37 °C and then removed. After further 24-h incubation, cell viability was estimated by conducting a modified MTT assay using Tetracolor ONE™. The percentage of damaged cells was calculated by setting non-treated cells as the control.

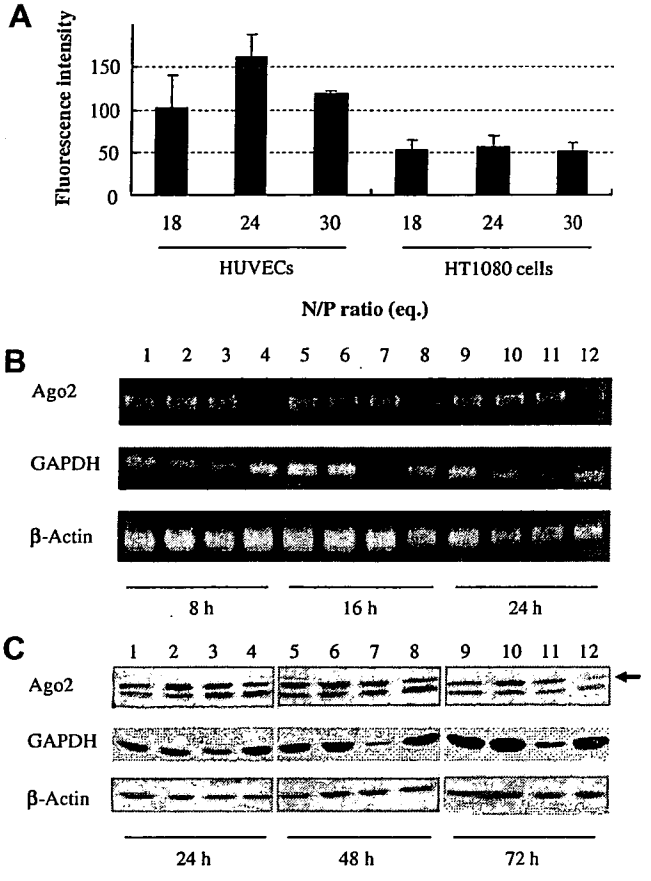

Fig. 2. Ago2 knockdown in HUVECs. (A) The amount of siRNA taken into HUVECs or HT1080 cells was determined after FAM-labeled siRNA/PCL complexes were allowed to interact with these cells for 4 h at 37 °C. PCLs composed of cetyl-PEI, DOPE, and cholesterol were prepared and mixed with FAM-labeled siRNA at the various *N/P* ratios indicated in the figure. The fluorescence intensities of FAM in the cells were corrected for protein content. (B) RT-PCR was performed by using HUVECs transfected with siAgo2 or siGAPDH. Total RNAs were isolated at 8, 16, and 24 h post-transfection, reverse transcribed, and applied to PCR using an Ago2, GAPDH or β-actin primer set. The PCR products were visualized by ethidium bromide under UV illumination. Lanes 1, 5, and 9, control without siRNA; lanes 2, 6, and 10, SiEGFP used as a non-silencing control; lanes 3, 7, and 11, SiGAPDH used as a control siRNA; and lanes 4, 8, and 12, SiAgo2. (C) Western blotting was performed by using HUVECs transfected with siAgo2 or siGAPDH. Cell extracts were prepared at 24, 48 or 72 h post-transfection. Ten micrograms of total protein was separated and incubated with anti-Ago2 rabbit polyclonal antibody, anti-actin rabbit polyclonal antibody or anti-GAPDH mouse monoclonal antibody. SiEGFP was used as non-silencing control; and siGAPDH, as control siRNA. Arrow shows the location of Ago2 protein. Lanes 1, 5, and 9, control without siRNA; lanes 2, 6, and 10, SiEGFP used as a non-silencing control; lanes 3, 7, and 11, SiGAPDH used as a control siRNA; and lanes 4, 8, and 12, SiAgo2.

nylidene difluoride (PVDF) membrane (MILLIPORE, Billerica, MA). After having been blocked for 1 h at room temperature with 5% skim milk in Tris–HCl-buffered saline containing 0.1% Tween 20 (TTBS, pH 7.4), the membrane was incubated with a primary antibody (β-actin and GAPDH; 0.1 μg/ml, Ago2; 2 μg/ml) for 2 h at room temperature. Then, it was incubated with a peroxidase-conjugated secondary antibody at a dilution of 1:10,000 for 1 h at room temperature. Each sample was developed by using a chemiluminescent substrate (ECL; Amersham Biosciences).

Cell growth assay. HUVECs were seeded onto 24-well plates at the density of 5×10^4 cells/dish and transfected with siAgo2 or siEGFP complexed with PCLs. After 0-, 24- or 48-h incubation, Tetracolor ONE™ was added to each well in accordance with the manufacturer's instructions. The amount of formazan formed in 2 h was measured by the microplate reader at a test wavelength of 492 nm and a reference wavelength of 630 nm.

Detection of apoptotic cells. HUVECs were seeded onto 35-mm dishes at the density of 2.5×10^5 cells/dish and transfected with siAgo2/ or siEGFP/PCL complexes. At 48 h after transfection, TUNEL staining was performed by using an ApopTag Plus Fluorescein In Situ Apoptosis Detection Kit (Chemicon International, Temecula, CA) according to the manufacturer's instructions. These cells were counterstained with DAPI and observed under an LSM510 META confocal Laser-Scanning-Microscope (Carl Zeiss, Oberkochen, Germany).

Tube formation assay. Matrigel (BD Biosciences Bedford, MA) was diluted to 4 mg/ml with EGM-2, added to 24-well plates, and allowed to undergo polymerization. HUVECs (5×10^5 cells/well) transfected with siAgo2 or siEGFP complexed with PCLs were then added to each well and incubated for 6 h at 37 °C. Photomicrographs were taken in 10 fields/group with an Olympus IMT-2 microscope (Olympus, Tokyo, Japan). The length of tubes was calculated by using software Image J (NIH, Bethesda, MD).

Results

Preparation of siRNA/PCLs complexes for siRNA delivery

At first, the adequate formulation of PCLs for siRNA transfection was determined by evaluating the uptake amount of siRNA, the knockdown efficiency, and the cytotoxicity. The sizes of siRNA/PCLs complexes prepared in this study were in the range of 130–155 nm, and the ξ-potentials of them were 30–50 mV. The uptake experiment showed that the presence of cholesterol in PCLs enhanced the uptake amount of FAM-labeled siAgo2 into HT1080 cells (Fig. 1A). In addition, the highest siRNA uptake was achieved when the *N/P* ratio of siRNA/PCLs complex was 24 equivalents (equiv). In the quantitative knockdown experiment, the siRNA formulation most taken up by HT1080 cells also showed the maximal knockdown efficiency (Fig. 1B). The cytotoxicity of siRNA/PCLs complexes was much lower than that of LFA2K (Fig. 1C).

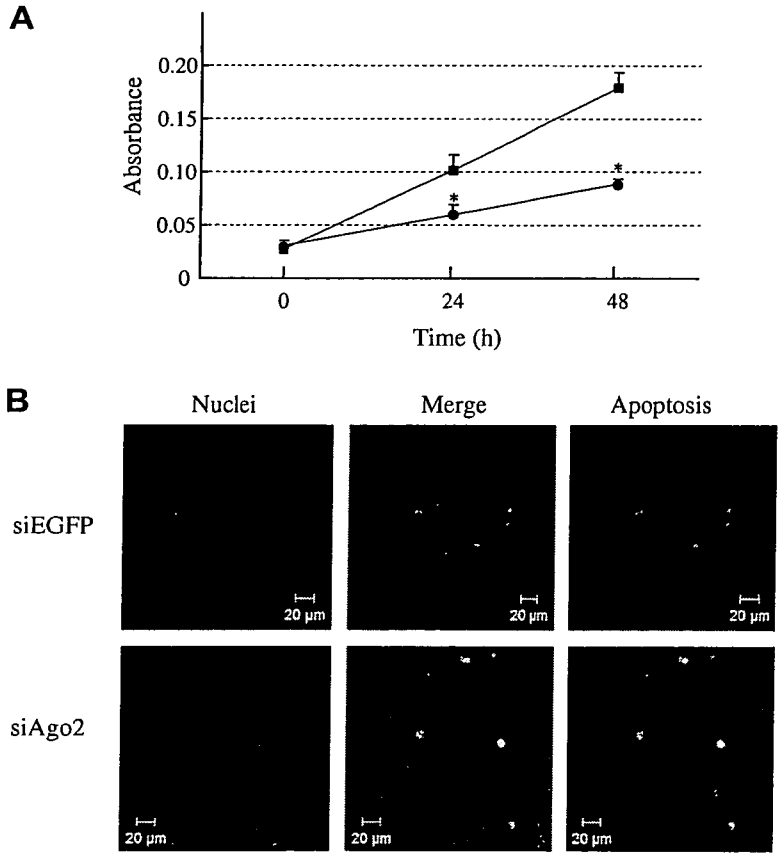

Fig. 3. Influence of Ago2 knockdown on the growth of HUVECs. (A) At 0, 24, and 48 h post-transfection, a modified MTT assay was performed with HUVECs transfected with siAgo2 (circles) or siEGFP (squares) complexed with PCLs. Data show the absorbance with SD bars. Significant differences from siEGFP group are indicated ($^*P < 0.01$). (B) Apoptosis of HUVECs transfected with siAgo2/PCL complexes was determined by TUNEL staining at 48 h post-transfection. The nuclei were counterstained with DAPI (blue). Apoptotic cells (FITC, green) were observed under an LSM510 META confocal Laser-Scanning-Microscope. Scale bars represent 20 μm.

Ago2 knockdown in HUVECs

To confirm Ago2 knockdown in HUVECs, these cells were transfected with siAgo2 (final concentration: 40 nM) complexed with PCLs. The uptake experiment indicated that the amount of FAM-labeled siAgo2 taken up was greater by HUVECs than by HT1080 cells (Fig. 2A). The optimal *N/P* ratio of siRNA/PCLs complexes for incorporating siRNA into HUVECs was 24 equiv, consistent with the result obtained for HT1080 cells. Based on these results from the formulation screening, we adopted the following formulation for use in subsequent experiments: cetyl-PEI/DOPE/cholesterol = 0.05/1/0.5 as a molar ratio, *N/P* ratio = 24 equiv. The RT-PCR data showed that siAgo2 down-regulated the expression of Ago2 mRNAs in HUVECs (Fig. 2B). The specificity of Ago2 knockdown was confirmed by the transfection with siEGFP or siGAPDH. Neither siEGFP nor siGAPDH affected the expression of Ago2 mRNA, and siGAPDH suppressed the expression of GAPDH mRNA. These data indicate that the knockdown of Ago2 occurred in a siAgo2-dependent manner. The Western blotting data demonstrated that the expression of Ago2 protein was actually diminished by siAgo2 transfection (Fig. 2C).

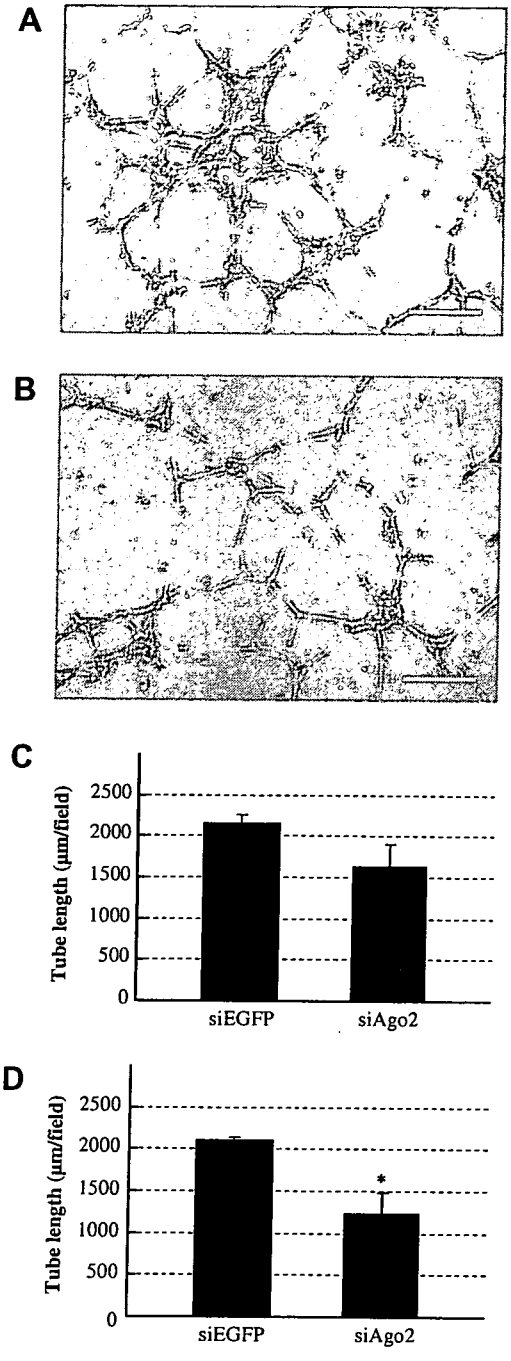

Fig. 4. Inhibition of tube formation by Argonaute2 knockdown. Tube formation assay was performed with HUVECs transfected with siAgo2/PCL complexes. The transfected cells were collected at 24 (C) or 48 h (A, B, and D) post-transfection and incubated on Matrigel for 6 h at 37 °C in 5% CO_2. (A, B) Photomicrographs show the tube formation of HUVECs transfected with siEGFP (A) or siAgo2 (B). Scale bars represent 20 μm. (C and D) The length of tubes was calculated by using the software Image J. Significant difference from siEGFP group is indicated ($^*P < 0.05$).

Influence of Ago2 knockdown on angiogenic potentials of HUVECs

To investigate the influence of Ago2 knockdown on the properties of endothelial cells, HUVECs were transfected with siAgo2/PCL complexes. The influence of Ago2 knockdown on the proliferation of HUVECs was determined by using a modified MTT assay. As shown in Fig. 3A, the treatment with siAgo2 significantly suppressed the growth of HUVECs in comparison to that with siEGFP, a control siRNA ($P < 0.001$). TUNEL staining showed that a certain population of HUVECs treated with siAgo2 underwent apoptosis at 48 h after the transfection (Fig. 3B). The percentage of apoptotic cells was about 20% in siAgo2-treated HUVECs. This result indicates that the growth inhibition by Ago2 knockdown was partially caused by the induction of apoptosis. On the other hand, Ago2 knockdown did not induce apoptosis of HT1080 cells in the similar experiment (Supplementary Fig. 1).

In the tube formation assay, the HUVECs transfected with siEGFP formed capillary-like structures (Fig. 4A). In contrast, the treatment with siAgo2 suppressed the tube formation of HUVECs (Fig. 4B). The length of tubes, an indicator of tube formation, was significantly reduced by the knockdown of Ago2 when HUVECs were used for this assay at 48 h post-transfection (Fig. 4C and D). These results indicate that siAgo2 inhibited indispensable events of angiogenesis.

Discussion

In the present study, we demonstrated that the knockdown of Ago2 resulted in the loss of the angiogenic potential of HUVECs, thus suggesting that Ago2 is required for angiogenesis. We consider one of the reasons to be indirect effects related to the miRNA system. The knockdown of Ago2 could affect the expression levels of some critical miRNAs required for the formation of angiogenic vessels.

For instance, it was reported that miR-221 and miR222 control the ability of HUVECs to form new capillaries [12]. However, the knockdown of Ago2 is considered to affect most miRNAs not just miR-221/2. As well as the knockdown of Ago2, the deletion of Dicer function resulted in failure of mouse embryonic angiogenesis [13]. These results indicate that the miRNA system is indispensable for angiogenesis, in which Ago2 also plays a critical role.

Angiogenesis is a crucial event for many severe diseases such as cancer. Therefore, the development of antiangiogenic RNAi therapy have been widely investigated [3]. The knockdown of angiogenic factor such as vascular endothelial growth factor is expected to be a novel therapeutic strategy [3]. Our data suggest that Ago2 might be a unique therapeutic target for antiangiogenic RNAi therapy. Since siAgo2 not only cleaves the mRNA of Ago2 but also occupies the protein of Ago2 that is required for RNAi, the use of siAgo2 is considered to be an efficient strategy to disturb an ordered miRNA system. The amount of Ago2 protein would not be rate determining in this strategy, whereas other siRNA requires sufficient Ago2 protein. Therefore, the knockdown of Ago2 is a unique approach for inhibiting angiogenesis. However, a siRNA delivery system that targets endothelial cells specifically is necessary to apply siAgo2 for antiangiogenic therapy, since siAgo2 would be expected to affect the entire miRNA system.

In the present study, we determined the optimal formulation of PCLs by determining the gene silencing efficiency and cytotoxicity and demonstrated PCLs to be a novel siRNA vector. PCLs carrying siAgo2 attenuated the angiogenic potential of HUVECs. In the case that PCLs carrying siAgo2 are applied *in vivo*, the availability of them will be extended by surface modification of the liposomes with functional molecules such as polyethyleneglycol and certain ligands targeting angiogenic endothelial cells. In our previous study, we demonstrated that Ala-Pro-Arg-Pro-Gly (APRPG) is a useful peptide for the active targeting of angiogenic vessels [17]. APRPG-modified liposomal doxorubicin actually caused effective tumor growth suppression through damaging angiogenic endothelial cells [17]. APRPG-modified liposomal siAgo2 might thus be a good candidate for use in antiangiogenic RNAi therapy.

Acknowledgments

This research was supported by Research on Advanced Medical Technology on Health and Labour Sciences Research Grants, Ministry of Health, Labour and Welfare, Japan.

Appendix A. Supplementary data

Supplementary data associated with this article can be found, in the online version, at doi:10.1016/j.bbrc.2008.01.074.

References

[1] A. Fire, S. Xu, M.K. Montgomery, S.A. Kostas, S.E. Driver, C.C. Mello, Potent and specific genetic interference by double-stranded RNA in *Caenorhabditis elegans*, Nature 391 (1998) 806–811.
[2] S.M. Elbashir, J. Harborth, W. Lendeckel, A. Yalcin, K. Weber, T. Tuschl, Duplexes of 21-nucleotide RNAs mediate RNA interference in cultured mammalian cells, Nature 411 (2001) 494–498.
[3] S.I. Pai, Y.Y. Lin, B. Macaes, A. Meneshian, C.F. Hung, T.C. Wu, Prospects of RNA interference therapy for cancer, Gene Ther. 13 (2006) 464–477.
[4] R.I. Gregory, T.P. Chendrimada, N. Cooch, R. Shiekhattar, Human RISC couples microRNA biogenesis and posttranscriptional gene silencing, Cell 123 (2005) 631–640.
[5] K. Okamura, A. Ishizuka, H. Siomi, M.C. Siomi, Distinct roles for Argonaute proteins in small RNA-directed RNA cleavage pathways, Genes Dev. 18 (2004) 1655–1666.
[6] J. Liu, M.A. Carmell, F.V. Rivas, C.G. Marsden, J.M. Thomson, J.J. Song, S.M. Hammond, L. Joshua-Tor, G.J. Hannon, Argonaute2 is the catalytic engine of mammalian RNAi, Science 305 (2004) 1437–1441.
[7] G. Meister, M. Landthaler, A. Patkaniowska, Y. Dorsett, G. Teng, T. Tuschl, Human Argonaute2 mediates RNA cleavage targeted by miRNAs and siRNAs, Mol. Cell 15 (2004) 185–197.
[8] C. Matranga, Y. Tomari, C. Shin, D.P. Bartel, P.D. Zamore, Passenger-strand cleavage facilitates assembly of siRNA into Ago2-containing RNAi enzyme complexes, Cell 123 (2005) 607–620.
[9] M. Cristofanilli, C. Charnsangavej, G.N. Hortobagyi, Angiogenesis modulation in cancer research: novel clinical approaches, Nat. Rev. Drug Discov. 1 (2002) 415–426.
[10] K. Shimizu, T. Asai, N. Oku, Antineovascular therapy, a novel antiangiogenic approach, Expert Opin. Ther. Targets 9 (2005) 63–76.
[11] N. Ferrara, K.J. Hillan, W. Novotny, Bevacizumab (Avastin), a humanized anti-VEGF monoclonal antibody for cancer therapy, Biochem. Biophys. Res. Commun. 333 (2005) 328–335.
[12] L. Poliseno, A. Tuccoli, L. Mariani, M. Evangelista, L. Citti, K. Woods, A. Mercatanti, S. Hammond, G. Rainaldi, MicroRNAs modulate the angiogenic properties of HUVECs, Blood 108 (2006) 3068–3071.
[13] W.J. Yang, D.D. Yang, S. Na, G.E. Sandusky, Q. Zhang, G. Zhao, Dicer is required for embryonic angiogenesis during mouse development, J. Biol. Chem. 280 (2005) 9330–9335.
[14] R.C. Ryther, A.S. Flynt, J.A. Phillips 3rd, J.G. Patton, siRNA therapeutics: big potential from small RNAs, Gene Ther. 12 (2005) 5–11.
[15] N. Oku, Y. Yamazaki, M. Matsuura, M. Sugiyama, M. Hasegawa, M. Nango, A novel non-viral gene transfer system, polycation liposomes, Adv. Drug Deliv. Rev. 52 (2001) 209–218.
[16] S. Yamakawa, Y. Furuyama, N. Oku, Development of a simple cell invasion assay system, Biol. Pharm. Bull. 23 (2000) 1264–1266.
[17] N. Oku, T. Asai, K. Watanabe, K. Kuromi, M. Nagatsuka, K. Kurohane, H. Kikkawa, K. Ogino, M. Tanaka, D. Ishikawa, H. Tsukada, M. Momose, J. Nakayama, T. Taki, Anti-neovascular therapy using novel peptides homing to angiogenic vessels, Oncogene 21 (2002) 2662–2669.

Chronopharmacologic Cancer Treatment with an Angiogenic Vessel-Targeted Liposomal Drug

Kosuke SHIMIZU,[a] Yasuharu SAWAZAKI,[a] Toshiki TANAKA,[b] Tomohiro ASAI,[a] and Naoto OKU*,[a]

[a] *Department of Medical Biochemistry, University of Shizuoka School of Pharmaceutical Sciences; 52–1 Yada, Suruga-ku, Shizuoka 422–8526, Japan: and* [b] *Department of Applied Chemistry, Faculty of Engineering, Nagoya Institute of Technology; Gokiso-cho, Nagoya 466–8555, Japan.* Received June 5, 2007; accepted September 27, 2007

Antineovascular therapy (ANET), which eradicates angiogenic endothelial cells by specifically delivered anticancer drugs to tumor cells to obtain complete cutoff of blood supply, is an effective modality for cancer treatment. Since the expression of vascular endothelial growth factor (VEGF) in hypoxic tumor cells is known to fluctuate in a circadian oscillation, we investigated the chronopharmacologic treatment of tumors with ANET. Adriamycin-encapsulated liposomes modified with the Ala-Pro-Arg-Pro-Gly (APRPG) peptide (APRPG-LipADM) were prepared, after the APRPG peptide had been shown to have affinity to angiogenic sites. Colon 26 NL-17 tumor-bearing mice were injected three times with APRPG-LipADM at Zeitgeber time (ZT) 2, 8, 14, and 20 where ZT 0 was the time lights were turned on, and tumor growth was monitored. Tumor growth suppression changed with dosing time and was significantly ($p<0.01$) more potent at ZT 14 compared with ZT 20. The VEGF concentration in the plasma of the tumor-bearing mice was higher in the light phase compared with that in the dark phase, and this circadian oscillation was related to dosing time dependency with ANET. These results indicate that tumor growth suppression is correlated to some extent with the VEGF concentration in the plasma, and that chronopharmacologic treatment of cancer with ANET may enhance the therapeutic efficacy and reduce the side effects.

Key words vascular endothelial growth factor; tumor angiogenesis; antineovascular therapy; liposome; circadian rhythm; drug delivery system

Tumor cells demand oxygen and nutrients, and tumor angiogenesis is critical for the growth and maintenance of solid tumors.[1—3] Therefore antiangiogenic inhibitors for cancer treatment have been developed.[4,5] Angiogenesis is promoted by various proangiogenic factors such as vascular endothelial growth factor (VEGF) that stimulate endothelial cell proliferation and sprouting to form vascular construction.[6] Antibodies against VEGF or VEGF receptor, kinase insert domain-containing receptor/fetal liver kinase-1 (KDR/flk-1), are known to inhibit angiogenesis effectively and to suppress tumor growth. The humanized monoclonal anti-VEGF antibody bevacizumab (Avastin) has been used clinically.[7,8] A peptide with the sequence Ala-Thr-Trp-Leu-Pro-Pro-Arg (ATWLPPR) inhibits VEGF binding to the receptor and also inhibits angiogenesis.[9] Antiangiogenic therapies based on the inhibition of the angiogenic cascade, however, may lead to tumor regression besides inducing tumor dormancy.[10]

We previously developed a novel antiangiogenic therapy, antineovascular therapy (ANET), in which angiogenic endothelial cells are targeted and damaged by chemotherapeutic agents.[11,12] Since angiogenic endothelial cells are proliferating during angiogenesis, they are susceptible to anticancer agents. Therefore we focused on delivering anticancer drugs to the angiogenic endothelial cells and eradicating them to obtain complete cutoff of blood supply to tumor cells. Although this therapy potentially has side effects due to the usage of cytotoxic anticancer agents, these side effects might be decreased by drug delivery system (DDS) technology. For this purpose, we first isolated peptides specific for angiogenic vasculature by *in vivo* biopanning using a phage-displayed 15-mer-peptide library.[11] As an epitope, we obtained the Ala-Pro-Arg-Pro-Gly (APRPG) peptide that specifically interacts with an angiogenic site. The APRPG peptide was then used for the modification of liposome, an active-targeting drug carrier. We previously observed that APRPG-modified liposome (APRPG-Lip) predominantly accumulated in tumor tissue and bound to VEGF-stimulated endothelial cells *in vitro*. When anticancer drugs such as adriamycin (ADM) are encapsulated in APRPG-Lip, it inhibits angiogenesis in dorsal air sac model mice, suppresses tumor growth with reduced side effects, and lengthens the survival time of tumor-bearing mice. ANET was effective in the drug-resistant tumor model.[13] Confocal microscopic observation and histochemical staining demonstrated that APRPG is applicable to human cancer.[11]

Koyanagi and coworkers reported that the expression of VEGF in hypoxic tumor cells fluctuated in a circadian oscillation[14]: The mRNA level of VEGF in implanted tumor cells was high at Zeitgeber time (ZT) 2 to 10, and low at ZT 14 to 18, and actual VEGF concentrations in plasma and tumor correspondingly oscillated. Furthermore, they observed higher tumor growth suppression by three different types of antiangiogenic agents, SU1498, TNP-470, and BB2516, at dosing time ZT 2 than at ZT 14 in sarcoma 180-bearing mice. After that elegant study, we attempted to investigate the chronopharmacologic treatment of tumors with ANET.

MATERIALS AND METHODS

Materials Stearoyl-APRPG derivative was synthesized as previously described.[15] Distearoylphosphatidylcholine (DSPC) was a gift from Nippon Fine Chemical Co., Ltd. (Takasago, Hyogo, Japan). Cholesterol was purchased from Sigma Chemical Co. (St. Louis, MO, U.S.A.).

Experimental Animals BALB/c male (3-week-old) mice were purchased from Japan SLC, Inc. (Shizuoka, Japan), housed under the standard laboratory conditions (23 °C and 55±5% humidity) and allowed access to tap water and food

* To whom correspondence should be addressed. e-mail: oku@u-shizuoka-ken.ac.jp

ad libitum. The mice were adapted to a 12-h light/dark cycle for 2 weeks before use. Lights were automatically turned on at 8:00 and off at 20:00, and ZT 0 indicates the time when lights were turned on. The animals were cared for according to the Animal Facility Guidelines of the University of Shizuoka.

Preparation of Liposomes Preparation of liposomes was performed as described previously.[11] In brief, DSPC and cholesterol with stearoyl-APRPG (10 : 5 : 1 as a molar ratio), or DSPC and cholesterol without APRPG derivative (10 : 5 as a molar ratio) were dissolved in chloroform, dried under reduced pressure, and stored *in vacuo* for at least 1 h. Liposomes were prepared by hydration of the thin lipid film with 0.3 M of citrate solution, pH 4.0, and frozen and thawed for three cycles using liquid nitrogen. Then, the liposomes were sized by extrusion three times through a polycarbonate membrane filter with 100-nm pores (Advantec, Tokyo, Japan). After adjusting the pH of the solution to pH 7.0 with sodium carbonate in HEPES buffer 20 mM, liposomes were incubated with ADM at 60 °C for 1 h, washed three times with PBS, and resuspended with glucose solution 0.3 M. Particle size of the liposomes was about 150 nm as recorded on an ELS-800 electrophoretic light-scattering spectrophotometer (Otsuka Electronics Co., Ltd., Osaka, Japan). The concentration of ADM was determined based on absorbance at 484 nm, and the encapsulation efficiency of ADM was greater than 90% throughout the experiment.

Therapeutic Experiment C26 NL-17 cells were cultured in RPMI1640 medium supplemented with 10% fetal bovine serum (FBS, Sigma) in a CO_2 incubator. After harvesting of the cells with 0.02% EDTA in PBS, 1.0×10^6 cells were carefully implanted subcutaneously into the posterior flank of 5-week-old male BALB/c mice. The mice were injected with Cont-LipADM or APRPG-LipADM intravenously *via* a tail vein (10 mg/kg as the dose of ADM) on day 18, when the tumor volumes became about 0.15 cm^3, with special care to minimize environmental changes. These liposomes were again administered on day 21 and 24 (30 mg/kg total ADM after three administrations, and about 0.045 mmol/kg liposomal dosage as DSPC in each injection). The dosing time of the sample on each day was determined to ZT 2, 8, 14, and 20, respectively. The size of tumors and the body weight of each mouse were monitored daily thereafter. Two bisecting diameters of each tumor were measured with slide calipers to determine the tumor volume, and calculation was performed using the formula 0.4 ($a\times b^2$), where a is the largest and b is the smallest diameter of the tumor. The tumor volume thus calculated correlated well with the actual tumor weight ($r=0.980$).[16]

ELISA for VEGF C26 NL-17-bearing mice were prepared as described above. On day 18 after tumor inoculation when the tumor volumes became about 0.15 cm^3, the mice ($n=4$) were killed under diethylether anesthesia and their blood was collected and centrifuged to obtain the plasma. The VEGF concentration in the plasma was determined using an ELISA (Mouse VEGF immunoassay, R&D Systems) according to the manufacturer's instructions. A standard curve was obtained with mouse VEGF. Absorbance at 562 nm was measured with a microplate reader, and the amount of VEGF was expressed as picograms per milliliter.

Statistical Analysis Variance in a group was evaluated using the F-test, and differences were evaluated with Student's t-test.

RESULTS

Chronopharmacologic Treatment of Tumors with ANET ZT 2, 8, 14, and 20 corresponded to 10:00, 16:00, 22:00, and 04:00, respectively since the lights were automatically turned on at 08:00 and off at 20:00. As shown in Fig. 1a, tumor growth was significantly ($p<0.01$) suppressed in all APRPG-LipADM groups. Among them, APRPG-LipADM was less potent for tumor growth suppression in the ZT 20 group, and a significant difference in tumor volume was observed between the ZT 20 group and ZT 14 group on days 34 and 35. As an indicator of side effects, we determined the body weight changes in the APRPG-LipADM groups and observed body weight loss in the ZT 2 and ZT 20 groups to some extent (Fig. 1b). The survival time was also monitored and the mean survival time for the control, ZT 2, ZT 8, ZT 14, and ZT 20 groups was 62.5, 77.4, 89.0, 77.8, and 73.2 d, respectively (Fig. 2). These data also indicate that APRPG-LipADM was less potent in the ZT 20 group, although it was also possible that the side effects shown as body weight loss in the ZT 20 group affected the life span.

Relationship between VEGF Concentration in Plasma and ANET Efficiency Since the suppression of tumor growth by APRPG-LipADM was affected by dosing time, the VEGF concentration in the plasma of C26 NL-17 tumor-

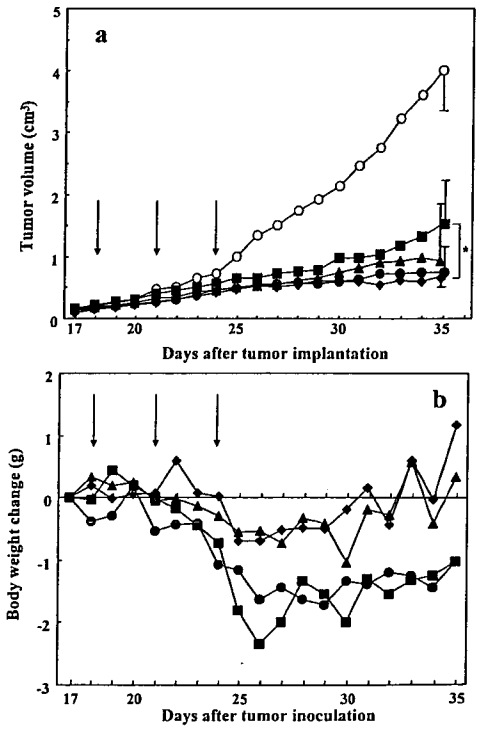

Fig. 1. Chronotherapy Using APRPG-LipADM against C26 NL-17 Carcinoma-Bearing Mice

C26 NL-17 carcinoma cells were subcutaneously implanted into BALB/c mice. The mice were intravenously administered glucose 0.3 M (○) or APRPG-LipADM (10 mg/kg/d as ADM) through a tail vein at ZT 2 (●), ZT 8 (▲), ZT 14 (◆), or ZT 20 (■) on days 18, 21, and 24 after tumor implantation. Tumor volume (a) and body weight change (b) in each mouse were measured to evaluate therapeutic effects. Data in (a) are presented as the mean tumor volume and S.D., where S.D. bars are shown only for the last points (day 35) for the sake of graphic clarity. Significant differences between APRPG-LipADM treated groups are indicated; $*p<0.05$. Arrows indicate the days of treatment.

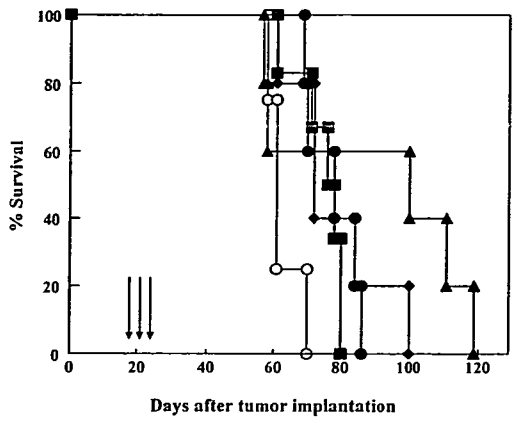

Fig. 2. Survival Time after Chronotherapy Using APRPG-LipADM in C26 NL-17 Carcinoma-Bearing Mice

C26 NL-17 carcinoma cells were subcutaneously implanted into BALB/c mice. The mice were intravenously administered glucose 0.3 M (○) or APRPG-LipADM (10 mg/kg/d as ADM) through a tail vein at ZT 2 (●), ZT 8 (▲), ZT 14 (◆), or ZT 20 (■) on days 18, 21, and 24 after tumor implantation. Arrows indicate the days of treatment.

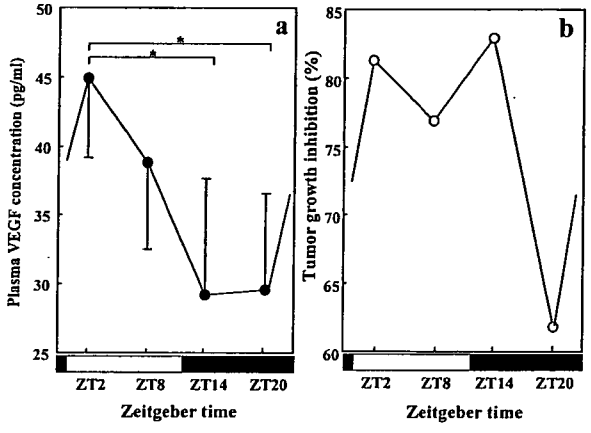

Fig. 3. Chronopharmacological Relationship between VEGF Concentration in the Plasma and Therapeutic Effect

a) C26 NL-17 carcinoma cells were subcutaneously implanted into BALB/c mice, and the mice were killed on day 18 at ZT 2 (●), ZT 8 (▲), ZT 14 (◆), or ZT 20 (■). Plasma VEGF concentration was determined as described in Materials and Methods. b) Tumor growth inhibition on day 35 was depicted based on Fig. 1 and arranged against ZT. Significant differences are indicated; $*p<0.05$.

bearing mice was determined at various ZTs. As shown in Fig. 3, the plasma VEGF concentration in the light phase was higher than that in the dark phase. This result is consistent with the previous study by Koyanagi and coworkers.[14] Figure 3 also shows the tumor volume on day 35 after tumor implantation, depicted from the data shown in Fig. 1. Tumor growth suppression was roughly correlated with the VEGF concentration in the plasma, although the decrease in tumor growth suppression was retarded in comparison with the decline in plasma VEGF concentration: Tumor growth was highly suppressed in the ZT 14 group, although the VEGF concentration was low at ZT 14. These data suggest that ANET was effective when the growth of tumor angiogenic endothelial cells was enhanced by VEGF, and the growth was retarded for several hours after stimulation with VEGF.

DISCUSSION

Tumor angiogenesis is critical for tumor growth and blood-borne metastasis. Therefore angiogenesis and angiogenic vessels have become a target for cancer treatment. Proangiogenic factors such as VEGF, angiopoietin, basic fibroblast growth factor, platelet-derived growth factor, and interleukin-8 may stimulate endothelial cells in a receptor-dependent manner and induce angiogenesis. The binding of VEGF to VEGF receptors initiates signal transduction in endothelial cells and these stimulated endothelial cells begin to proliferate and sprout to form neovessels. Therefore the inhibitors of VEGF binding or its signal transduction are thought to suppress tumor growth by blocking the neovessel formation that is critical for the supply of oxygen and nutrients to tumor cells. Traditional antiangiogenic therapy, however, is rather passive. Therefore we designed a modality for active degeneration of neovessel constructs, ANET.[11,12] In this modality, we deliver cytotoxic agents to angiogenic endothelial cells, which directly eradicate angiogenic vasculature, since cytotoxic agents damage the growing endothelial cells as well as tumor cells.

A number of living organisms including humans show periodicity in biologic functions. Recent studies have revealed that the circadian rhythm is regulated by several specific clock gene produces.[17—19] Circadian rhythm is known to affect various events in a body related to drug efficacy: The oscillation of sensitivity of target organs, drug metabolism, *etc.* changes the bioavailability and side effects of drugs. Therefore, in such cases, scheduling of dosing time enhances drug efficacy and reduces side effect.[20—23] Anticancer drugs are also chronologically considered for scheduling to reduce side effects and enhance antitumor activity.[24—28] These results indicate that the susceptibility of tumor cells to anticancer agents oscillates. Moreover, the efficacy of antiangiogenic therapy depends on dosing time,[14,29] since the previous report suggested that VEGF production also fluctuates in a circadian fashion.

In the present study, we chronologically treated tumors with ANET, since the therapeutic efficacy of ANET is affected by dosing time. As shown in Fig. 1, the therapeutic efficacy of APRPG-LipADM was dependent on the dosing time; it was potent at ZT 2 to ZT 14 and weak at ZT 20. The plasma VEGF concentration also fluctuated in a circadian fashion, consistent with the data of Koyanagi *et al.*[14] Considering these data, the oscillation of tumor growth inhibition by APRPG-LipADM may be explained as VEGF stimulates the growth of angiogenic endothelial cells, and the cells in growing phase are more susceptible to ADM. Thus the damaged endothelial cells caused regression of tumor growth. At ZT 14, the VEGF concentration in the plasma is low in the daily oscillation, although tumor regression due to treatment with APRPG-LipADM at ZT 14 was clear. We speculate that it took several hours from VEGF stimulation of angiogenic endothelial cells to the growth of the cells.

Alternatively, VEGF stimulation might augment the binding site of APRPG on the surface of angiogenic endothelial cells, enhancing the binding of APRPG-LipADM at ZT 2 to ZT 14. (The target molecule of APRPG, however, is not clear at present.) APRPG-Lip bound to human umbilical vein endothelial cells (HUVECs) when the cells had been stimulated with VEGF.[11] If this was the case, APRPG-Lip did not bind sufficiently at ZT 20 when the APRPG-binding site was less present on the surface of the endothelial cells. In Fig. 1b, the

side effect was slightly more potent at ZT 20 and ZT 2 than at ZT 8 and ZT 14. Although we do not speculate that the unbound APRPG-LipADM caused greater side effects, since the accumulated amount of APRPG-Lip in tumors was less than 2% of the injected dose per gram of tumor tissue.[11] To *et al.*[30] examined the dosing time dependency of doxorubicin-induced cardiotoxicity and bone marrow toxicity after repeated administration in rats. They reported that the toxic effects were significantly high in the 9 HALO-treated group, corresponding to ZT 9 and that the reason was the increased AUC of the drug.[30] The body weight change observed in Fig. 1b, however, is not explained by the results of To and coworkers, since the pharmacokinetics of free drug and liposomal drug are completely different.

In conclusion, chronopharmacological treatment of cancer with ANET promises enhanced therapeutic efficacy and reduced side effects. This dosing time dependency may be due, at least in part, by circadian oscillation of the plasma VEGF concentration.

Acknowledgment This work was supported in part by a Grant-in-Aid for Scientific Research from the Japan Society for the Promotion of Science.

REFERENCES

1) Folkman J., *Curr. Mol. Med.*, **3**, 643—651 (2003).
2) Hanahan D., Weinberg R. A., *Cell*, **100**, 57—70 (2000).
3) Kerbel R. S., *Semin. Oncol.*, **31**, 54—60 (2004).
4) Soria J. C., Fayette J., Armand J. P., *Ann. Oncol.*, **15** (Suppl. 4), 223—227 (2004).
5) Kerbel R., Folkman J., *Nat. Rev. Cancer*, **2**, 727—739 (2002).
6) Ferrara N., Gerber H. P., LeCouter J., *Nat. Med.*, **9**, 669—676 (2003).
7) Gerber H. P., Ferrara N., *Cancer Res.*, **65**, 671—680 (2005).
8) Kabbinavar F. F., Schulz J., McCleod M., Patel T., Hamm J. T., Hecht J. R., Mass R., Perrou B., Nelson B., Novotny W. F., *J. Clin. Oncol.*, **23**, 3697—3705 (2005).
9) Starzec A., Vassy R., Martin A., Lecouvey M., Di Benedetto M., Crepin M., Perret G. Y., *Life Sci.*, **79**, 2370—2381 (2006).
10) Shimizu K., Oku N., *Biol. Pharm. Bull.*, **27**, 599—605 (2004).
11) Oku N., Asai T., Watanabe K., Kuromi K., Nagatsuka M., Kurohane K., Kikkawa H., Ogino K., Tanaka M., Ishikawa D., Tsukada H., Momose M., Nakayama J., Taki T., *Oncogene*, **18**, 2662—2669 (2002).
12) Shimizu K., Asai T., Oku N., *Exp. Opin. Ther. Targets*, **9**, 63—76 (2005).
13) Shimizu K., Asai T., Fuse C., Sadzuka Y., Sonobe T., Ogino K., Taki T., Tanaka T., Oku N., *Int. J. Pharm.*, **296**, 133—141 (2005).
14) Koyanagi S., Kuramoto Y., Nakagawa H., Aramaki H., Ohdo S., Soeda S., Shimeno H., *Cancer Res.*, **63**, 7277—7283 (2003).
15) Asai T., Shimizu K., Kondo M., Kuromi K., Watanabe K., Ogino K., Taki T., Shuto S., Matsuda A., Oku N., *FEBS Lett.*, **520**, 167—170 (2002).
16) Oku N., Doi K., Namba Y., Okada S., *Int. J. Cancer*, **58**, 415—419 (1994).
17) van der Horst G. T. J., Muijtjens M., Kobayashi K., Takano R., Kanno S., Takao M., de Wit J., Verkerk A., Eker A. P. M., van Leenen D., Buijs R., Bootsma D., Hoeijmakers J. H. J., Yasui A., *Nature* (London), **398**, 627—630 (1999).
18) Merrow M., Spoelstra K., Roenneberg T., *EMBO Rep.*, **6**, 930—935 (2005).
19) Bell-Pedersen D., Cassone V. M., Earnest D. J., Golden S. S., Hardin P. E., Thomas T. L., Zoran M. J., *Nat. Rev. Genet.*, **6**, 544—556 (2005).
20) Ohdo S., Koyanagi S., Suyama H., Higuchi S., Aramaki H., *Nat. Med.*, **7**, 356—360 (2001).
21) Khedhaier A., Attia M. B., Gadacha W., Sani M., Bouzouita K., Chouchane L., Mechkouri M., Reinberg A., Boughattas N. A., *Chronobiol. Int.*, **20**, 1103—1116 (2003).
22) Yoshida M., Ohdo S., Kakane H., Tomiyoshi Y., Matsuo A., Yukawa E., Higochi S., *J. Pharmacol. Exp. Ther.*, **305**, 1200—1205 (2003).
23) Matsunaga N., Nakamura N., Yoneda N., Qin T., Terazono H., To H., Higuchi S., Ohdo S., *J. Pharmacol. Exp. Ther.*, **311**, 594—600 (2004).
24) Granda T. G., Filipski E., D'Attino R. M., Vrignaud P., Anjo A., Bissery M. C., Levi F., *Cancer Res.*, **61**, 1996—2001 (2001).
25) Gorbacheva V. Y., Kondratov R. V., Zhang R., Cherukuri S., Gudkov A. V., Takahashi J. S., Antoch M. P., *Proc. Natl. Acad. Sci. U.S.A.*, **102**, 3529—3530 (2005).
26) Li X. M., Tanaka K., Sun J., Filipski E., Kayitalire L., Focan C., Levi F., *Br. J. Cancer*, **92**, 1684—1689 (2005).
27) Tabuchi H., To H., Sakaguchi N., Goto A., Takeuchi S., Higuchi S., Ohdo S., *Cancer Res.*, **65**, 8448—8454 (2005).
28) Asao T., Sakurai H., Harashima K., Yamaguchi S., Tsutsumi S., Nonaka T., Shioya M., Nakano T., Kuwano H., *Int. J. Hyperthermia*, **22**, 399—406 (2006).
29) Koyanagi S., Nakagawa H., Kuramoto Y., Ohdo S., Soeda S., Shimeno H., *J. Pharmacol. Exp. Ther.*, **304**, 669—674 (2003).
30) To H., Ohdo S., Shin M., Uchimaru H., Yukawa E., Higuchi S., Fujimura A., Kobayashi E., *J. Pharm. Pharmacol.*, **55**, 803—810 (2003).

Available online at www.sciencedirect.com
ScienceDirect
ELSEVIER
International Journal of Pharmaceutics 353 (2008) 65–73
INTERNATIONAL JOURNAL OF PHARMACEUTICS
www.elsevier.com/locate/ijpharm

A metronomic schedule of cyclophosphamide combined with PEGylated liposomal doxorubicin has a highly antitumor effect in an experimental pulmonary metastatic mouse model

Emi Shiraga[a], Jose Mario Barichello[a,b], Tatsuhiro Ishida[a,*], Hiroshi Kiwada[a]

[a] *Department of Pharmacokinetics and Biopharmaceutics, Subdivision of Biopharmaceutical Science, Institute of Health Biosciences, The University of Tokushima, 1-78-1 Sho-machi, Tokushima 770-8505, Japan*
[b] *Japan Association for the Advancement of Medical Equipment, Tokyo 113-0033, Japan*

Received 10 August 2007; received in revised form 11 October 2007; accepted 10 November 2007
Available online 17 November 2007

Abstract

Metronomic chemotherapy is a novel approach to the control of advanced cancer, as it appears to preferentially inhibit endothelial cell activity in the growing vasculature of tumors. Doxorubicin-containing sterically stabilized liposomes (DXR-SL) accumulate in large amounts in tumor tissue, resulting in enhanced antitumor effects of the encapsulated DXR. In the present study, it was hypothesized that metronomic chemotherapy may further augment the accumulation of DXR-SL, improving its therapeutic efficacy. This study tests the antitumor efficacy for the combination of a metronomic cyclophosphamide (CPA)-dosing schedule with sequential intravenous injections of DXR-SL in the treatment of lung metastatic B16BL6 melanoma-bearing mice. Three dosing schedules for the combination of metronomic CPA injections (s.c. 170 mg/kg every 6 days) plus either a low or a high dose of DXR-SL (i.v. 1 or 5 mg/kg every 6 days) were set: Schedule I, DXR-SL was given 3 days before the first CPA treatment; Schedule II, DXR-SL and CPA were given simultaneously; and, Schedule III, DXR-SL was given 3 days after the first CPA treatment. Lung weight and median survival time (MST) were evaluated. As expected, both the dosing schedule as well as the dose of DXR-SL improved therapeutic efficacy. Schedule I with the low DXR dose and Schedule II with the low or high DXR dose significantly increased MST, compared with regular metronomic CPA therapy. Under the dosing schedules (Schedule I with the low DXR dose and Schedule II with the high DXR), there was a strong relationship between increased MST and decreased lung weight. However, Schedule I with high DXR dose resulted in significantly lower lung weights, but did not increase MST, suggesting that chemotherapy may result in increased toxicity in some conditions. Although treatment regimens require optimization, the results of the present study may prove useful in further explorations of combining metronomic chemotherapy with liposomal anticancer drugs in the treatment of solid tumors.

Keywords: Combination therapy; Metronomic chemotherapy; Liposomal anticancer drug; PEGylated liposome; Cyclophosphamide; Doxorubicin

1. Introduction

Traditionally, systemic anti-cancer therapy has been dominated by the use of cytotoxic chemotherapeutics, which often are administered as a single dose or in short courses of therapy using the maximum tolerated dose (MTD) (conventional chemotherapy). MTD chemotherapy requires prolonged breaks between successive cycles of therapy due to toxicity (Kerbel and Kamen, 2004). On the other hand, a novel chemotherapeutic regimen, metronomic chemotherapy, recently has been advocated (Kerbel and Kamen, 2004; Gille et al., 2005; Munoz et al., 2005; Laquente et al., 2007; Tonini et al., 2007). Metronomic chemotherapy refers to the frequent administration of

Abbreviations: CHOL, cholesterol; CPA, cyclophosphamide; DXR, doxorubicin; DXR-SL, DXR-containing PEGylated liposomes; EPR, enhanced permeability and retention; HEPC, hydrogenated egg phosphatidylcholine; MPS, mononuclear phagocyte system; $mPEG_{2000}$-DSPE, 1,2-distearoyl-*sn*-glycero-3-phosphoethanolamine-*n*-[methoxy (polyethylene glycol)-2000]; MST, median survival time; MTD, maximum tolerated dose; PEG, polyethylene glycol; TβR-I, transforming growth factor type I receptor; TSP-1, thrombospondin-1; WBC, white blood cells.

* Corresponding author. Tel.: +81 88 633 7260; fax: +81 88 633 7260.
E-mail address: ishida@ph.tokushima-u.ac.jp (T. Ishida).

0378-5173/$ – see front matter © 2007 Elsevier B.V. All rights reserved.
doi:10.1016/j.ijpharm.2007.11.020

chemotherapeutics at doses significantly below the MTD without prolonged drug-free breaks. The therapy shows lower toxicity, allowing prolonged treatment.

The target of metronomic chemotherapy is believed to be the genetically stable endothelial cells within the vascular bed of the tumor, rather than tumor cells with a high rate of mutations (Browder et al., 2000). Thus, this strategy is categorized as an anti-angiogenic chemotherapy (Browder et al., 2000; Kerbel and Kamen, 2004; Munoz et al., 2005; Laquente et al., 2007; Tonini et al., 2007). Various chemotherapeutics, such as cyclophosphamide (CPA), vinblastine, methotrexate, etoposide and tegafur, are used for metronomic chemotherapy (Klement et al., 2000, 2002; Bello et al., 2001; Shaked et al., 2005; Klink et al., 2006; Munoz et al., 2006); among these, CPA is most frequently used. CPA is traditionally used for chemotherapy as an alkylating agent, which kills the tumor cells directly. However, it is reported that at lower doses, CPA enhances expression of thrombospondin-1 (TSP-1) in stromal and tumor cells (Hamano et al., 2004). TSP-1, a component of the extracellular matrix, which is secreted and found in circulation, is a well-known endogenous inhibitor of angiogenesis (de Fraipont et al., 2001; Lawler, 2002). The molecule primarily binds to CD36 receptors, which are expressed by endothelial cells of tumors (Dawson et al., 1997). It is thought that this interaction blocks proliferation and induces apoptosis in tumor endothelial cells, thereby inducing collapse of angiogenic vessels (Dawson et al., 1997; Guo et al., 1997; Jimenez et al., 2000). Consequently, metronomic CPA-dosing reduces tumor neovascularization, thus suppressing tumor growths (Browder et al., 2000; Kerbel and Kamen, 2004).

Chemotherapy delivered in nanocarriers has been developed to improve the clinical treatment of solid tumors by achieving high accumulation of chemotherapeutic agents in tumor tissues but limited accumulation in healthy organs. Doxil, doxorubicin-containing sterically stabilized (PEGylated) liposomes, is one such drug that has already been used clinically (Grunaug et al., 1998; Safra et al., 2000; Krown et al., 2004). It is well-known that sterically stabilized (PEGylated) liposomes (SL) show prolonged circulating times as a result of reduced opsonization by serum proteins and lowered recognition by cells of the mononuclear phagocyte system (MPS) (Lasic et al., 1991; Torchilin et al., 1994). Consequently, SL accumulate in solid tumors via angiogenic blood vessels that have increased permeability (Jain, 1987; Papahadjopoulos et al., 1991; Wu et al., 1993; Yuan et al., 1995; Forssen et al., 1996; Vaage et al., 1997), due to the so-called "enhanced permeability and retention (EPR) effect" (Maeda et al., 2000). As described above, metronomic injection of low-dose CPA induces the collapse of tumor angiogenic vessels. This may enhance the EPR effect for SL, resulting in increased nanocarrier accumulation in tumor tissue. The use of metronomic CPA chemotherapy combined with DXR-SL may thus have clinical significance and practical importance in treating solid tumors.

Therefore, the objective of the present study was to determine whether the combination of metronomic cyclophosphamide (CPA)-administration and sequential intravenous injections of DXR-SL improves antitumor efficacy in lung metastatic B16BL6 melanoma-bearing mice. The results indicated that a combination approach may improve therapeutic efficacy under some dosage regimens, although this approach is accompanied by an increase in toxicity.

2. Materials and methods

2.1. Materials

Hydrogenated egg phosphatidylcholine (HEPC) and 1,2-distearoyl-*sn*-glycero-3-phosphoethanolamine-*n*-[methoxy (polyethylene glycol)-2000] (mPEG$_{2000}$-DSPE) were generously donated by Nippon Oil and Fat (Tokyo, Japan). Doxorubicin (DXR) was generously donated by Daiichi Pharmaceutical. (Tokyo, Japan). Cholesterol (CHOL) and cyclophosphamide (CPA) were purchased from Wako Pure Chemical (Osaka, Japan). FITC-labeled rabbit anti-rat IgG heavy and light chain polyclonal antibody was purchased from Abcam (Cambridge, UK). Rat monoclonal anti-mouse CD45 antibody was purchased from R&D systems (CA, USA). All other reagents were of analytical grade.

2.2. Animal and tumor cell line

Male C57BL/6 mice, 5 weeks old, were purchased from Japan SLC (Shizuoka, Japan). The experimental animals were allowed free access to water and mouse chow, and were housed under controlled environmental conditions (constant temperature, humidity, and 12 h dark–light cycle). All animal experiments were evaluated and approved by the Animal and Ethics Review Committee of the University of Tokushima.

The pulmonary metastatic mouse melanoma cell line, B16BL6, was maintained in DMEM (Wako Pure Chemical) supplemented with 10% heat-inactivated FBS (Japan Bioserum, Hiroshima, Japan), 10 mM L-glutamine, 100 units/ml penicillin and 100 μg/ml streptomycin in a 5% CO_2 air incubator at 37 °C.

2.3. Preparation of liposomes

PEGylated liposomes (sterically stabilized liposomes, SL) were composed of HEPC/CHOL/mPEG$_{2000}$-DSPE (2/1/0.1 molar ratio). Liposomes were prepared using the thin-film hydration technique (Ishida et al., 2003). Briefly, the lipids were dissolved in chloroform and, after evaporation of the organic solvent, the resulting lipid film was hydrated with 250 mM ammonium sulfate solution (pH 5.5). The liposomes were sized by subsequent extrusion through polycarbonate membrane filters (Nuclepore, CA, USA) with pore sizes of 400, 200, and 100 nm. The mean diameter of the liposomes was approximately 100 nm, as determined using a NICOMP 370 HPL submicron particle analyzer (Particle Sizing System, CA, USA). The phospholipid concentration was determined by colorimetric assay (Bartlett, 1959). DXR was encapsulated into the liposomes by remote loading using an ammonium sulfate gradient, as previously described (Bolotin et al., 1994). Following extrusion, the external buffer was exchanged by eluting through a Sephadex G-50 column equilibrated with 10% sucrose. DXR was dissolved in a sucrose solution at a concentration of 10 mg/ml.

The DXR solution then was added to the liposome solution at a concentration of 0.2 mg DXR/1 mg phospholipid. The mixture was incubated in a 65 °C water bath for 1 h with slow agitation. After loading DXR into the liposomes, unencapsulated DXR was removed using a Sephadex G-50 column in HEPES buffered saline (25 mM HEPES, 140 mM NaCl, pH 7.4). DXR-loading efficiency was >90%.

2.4. In vivo assessment of tumor growth

B16BL6 cells were grown to 80–90% confluence in a 10 cm culture dish, harvested, and resuspended in cold PBS (51 mM Na_2HPO_4, 12 mM NaH_2PO_4, 77 mM NaCl, pH 7.4). The cells (5×10^4) in 0.2 ml PBS were inoculated into the tail vein of C57BL/6 mice.

CPA and DXR treatments were started 14 days after inoculating the mice with B16BL6 cells, because our earlier study demonstrated that extensive progression of tumor nodules on the surface of the lungs was evident 14 days post-inoculation (Li et al., 2005). The antitumor effect of the treatments was evaluated by survival time and lung weight at time of death. Body weight also was evaluated as a surrogate marker of toxicity.

2.5. CPA and DXR-SL dosing schedules

The CPA and DXR-SL treatments were as follows:

(1) *Conventional dosing of CPA*. Mice ($n = 5$) received two cycles of CPA treatment separated by a 3-week interval. Each cycle consisted of a total of three doses of CPA (150 mg/kg per dose) administered subcutaneously every other day (total dose of 450 mg/kg, i.e., MTD, maximum tolerated dose) (Browder et al., 2000).
(2) *Metronomic dosing of CPA*. Mice received eight doses of CPA (170 mg/kg per dose) administered subcutaneously at 6-day intervals (Browder et al., 2000).
(3) *Conventional dosing of DXR-SL*. Mice received DXR-SL (1 or 5 mg/kg) intravenously at 6-day intervals until the mice died.
(4) *Combination dosing of CPA with DXR-SL:*
    (i) *Schedule I (low or high dose of DXR-SL)*. CPA (170 mg/kg) was administered subcutaneously at 6-day intervals. Three days *before* CPA injection (11 day after tumor inoculation), high (5 mg/kg) and low (1 mg/kg) dose DXR-SL administered intravenously at 6-day intervals.
    (ii) *Schedule II (low or high dose of DXR-SL)*. CPA (170 mg/kg) was administered subcutaneously and high (5 mg/kg) or low (1 mg/kg) dose DXR-SL intravenously at 6-day intervals. The treatment was started at day 14 after tumor inoculation.
    (iii) *Schedule III (low or high dose of DXR-SL)*. CPA (170 mg/kg) was administered subcutaneously at 6-day intervals. Three days *after* the first CPA injection (17 day after tumor inoculation), high (5 mg/kg) or low (1 mg/kg) DXR-SL was administered intravenously and the injections were continued at 6-day intervals.

2.6. Toxicity assessment

To avoid the influence of tumorigenesis on toxicity assessment, normal C57BL/6 mice were used. Mice received six cycles of CPA or DXR-SL treatment administered at 6-day intervals. One cycle consisted of either subcutaneous administration of CPA (170 mg/kg) or intravenous injection of DXR-SL (1 or 5 mg/kg). After treatment was initiated, body weight was measured every 3 days. To determine change in the number of circulating white blood cells (WBC), blood was collected via retro-orbital puncture 7, 19 and 31 days after treatment was begun. Blood samples were washed twice with cold PBS and blood cells were collected by centrifugation for 5 min at 2000 rpm and 4 °C. Blood cells were blocked with 1% BSA/PBS for 15 min at room temperature and then were incubated with primary antibody (rat monoclonal anti-mouse CD45 antibody) for 30 min. After washing with cold PBS, samples were incubated for an additional 30 min with secondary antibody (FITC-labeled rabbit anti-rat IgG heavy- and light-chain polyclonal antibody). WBC number was determined using flow cytometry (Guava EasyCyte Mini System, GE Healthcare, CA, USA).

2.7. Statistics

All values are expressed as the mean ± S.D. Statistical analysis was performed with a two-tailed unpaired t-test using GraphPad InStat software (GraphPad Software, CA, USA). The level of significance was set at $p < 0.05$.

3. Results

3.1. Antitumor effect of a metronomic CPA-dosing schedule on pulmonary metastatic B16BL6 melanoma-bearing mice

The pulmonary metastatic B16BL6 melanoma bearing mouse model was employed in the present study because the antitumor effects of metronomic CPA chemotherapy have not yet been reported for a plumonary metastatic model. Conventional and metronomic CPA-dosing schedules significantly improved median survival time (MST) of tumor-bearing mice compared with controls (no-treatment). In addition, the metronomic schedule remarkably prolonged MST compared with the conventional schedule (control = 24.0 days, conventional schedule = 36.5 days and metronomic schedule = 50.0 days) (Fig. 1A). In experimental pulmonary metastasis models, lung weight reflects the growth of pulmonary metastases (Fig. 1B). Conventional and metronomic CPA-dosing schedules significantly inhibited the growth of cells that had metastasized to the lungs compared with control (no-treatment). Moreover, the metronomic schedule was significantly more efficient than the conventional schedule (Fig. 1B). Throughout these experiments, animals did not exhibit significant weight loss (data not shown). These results confirmed that the metronomic CPA-dosing schedule is more effective than the conventional dosing schedule with no severe side effects in lung metastatic B16BL6 melanoma-bearing mice. In contrast, when the dosing was started 3 days after B16BL6 cell-inoculation, lung weights

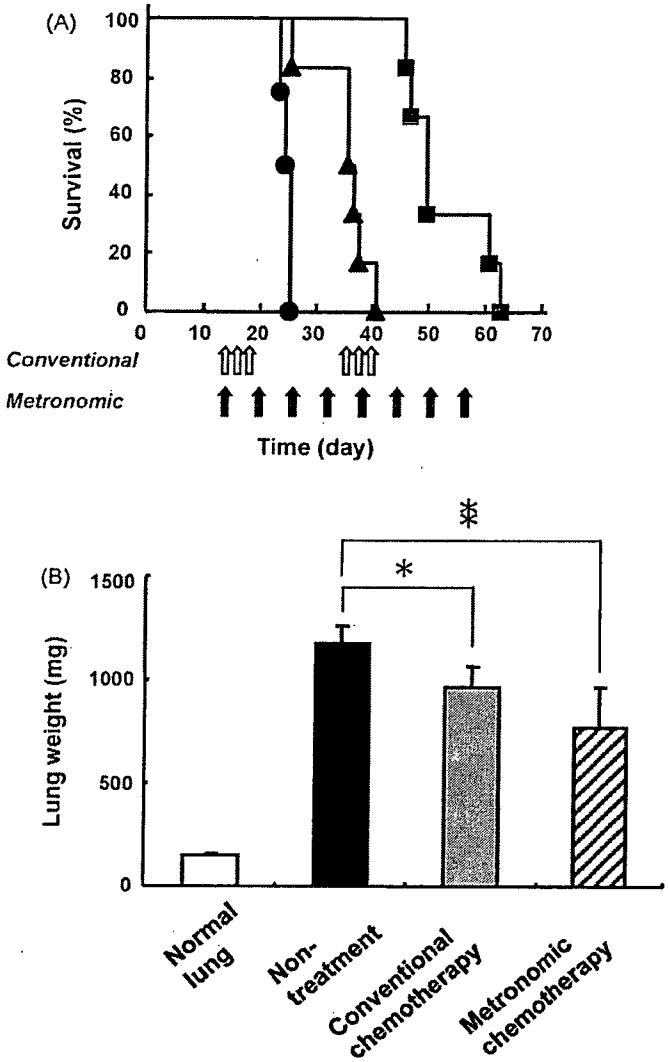

Fig. 1. Effect of either conventional (maximum tolerated dose) or metronomic CPA-dosing on (A) survival of B16BL6-bearing mice and (B) lung weight at time of death. Control (no treatment (●), conventional dosing (▲), 2 cycles consisting of 3 doses (white arrows) of 150 mg/kg administered every other day (total 450 mg/kg) with 3 weeks between cycles. Metronomic dosing (■), 8 doses of 170 mg/kg (black arrows) administered at 6-day intervals. $N=5$ mice per group. $^{*}p<0.05$; $^{**}p<0.005$ vs. control.

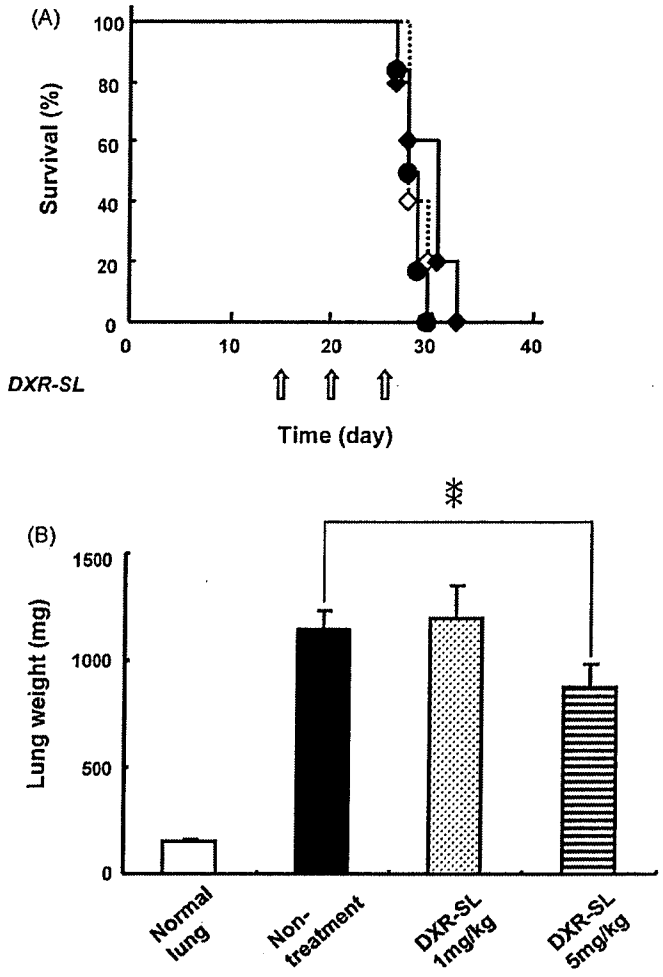

Fig. 2. Effect of DXR-SL (high or low dose) on (A) survival of B16BL6-bearing mice and (B) lung weight at time of death. Control (●). DXR-SL (◇ with dotted line), 3 doses of 1 mg/kg administered at 6-day intervals. DXR-SL (♦), 3 doses of 5 mg/kg administered at 6-day intervals. $N=5$ mice per group. $^{**}p<0.005$ vs. control.

did not increase, regardless of which CPA-dosing schedule was used. No tumor nodules were evident on the surface of lungs (data not shown). Thus, when the growth and formation of pulmonary metastases were minimal, because only 3 days had passed since inoculation with melanoma cells, both schedules had remarkable therapeutic efficiency in this animal model.

3.2. Antitumor effect of sequential DXR-SL administration on pulmonary metastatic B16BL6 melanoma bearing mice

Two different doses of DXR-SL (low and high) were administered intravenously every 6 days, 3 cycles, into tumor bearing mice from 14 day after tumor cells-inoculation. No significant increases in the MST were observed for either DXR-SL dose when administered according to a conventional dosing schedule (Fig. 2A): MSTs of control (no-treatment), low and high DXR-SL doses were 28.4, 29.0 and 32.0 days, respectively. However, lung weights of tumor-bearing mice indicated that the higher DXR-SL dose slightly inhibited the growth of metastasized cells (Fig. 2B). These findings demonstrate that sequential administration of DXR-SL had a very mild antitumor effect, although the effect did not appear to be related to extension of survival time in tumor-bearing mice. Throughout this experiment, no significant weight loss was observed (data not shown).

3.3. Antitumor effect of the combination of a metronomic CPA-dosing schedule and sequential administration of DXR-SL

To examine the effect of the combination therapy, CPA was metronomically administered either alone or plus DXR-SL (low or high dose). Sequential administration of DXR-SL (every 6 days) was started either 3 days before (Schedule I), on the same day as (Schedule II), or 3 days after (Schedule III), the first CPA injection because the metronomic CPA-dosing schedule may have affected the accumulation of SL in tumor tissue by increasing the permeability of angiogenic blood vessels. Schedules I, II

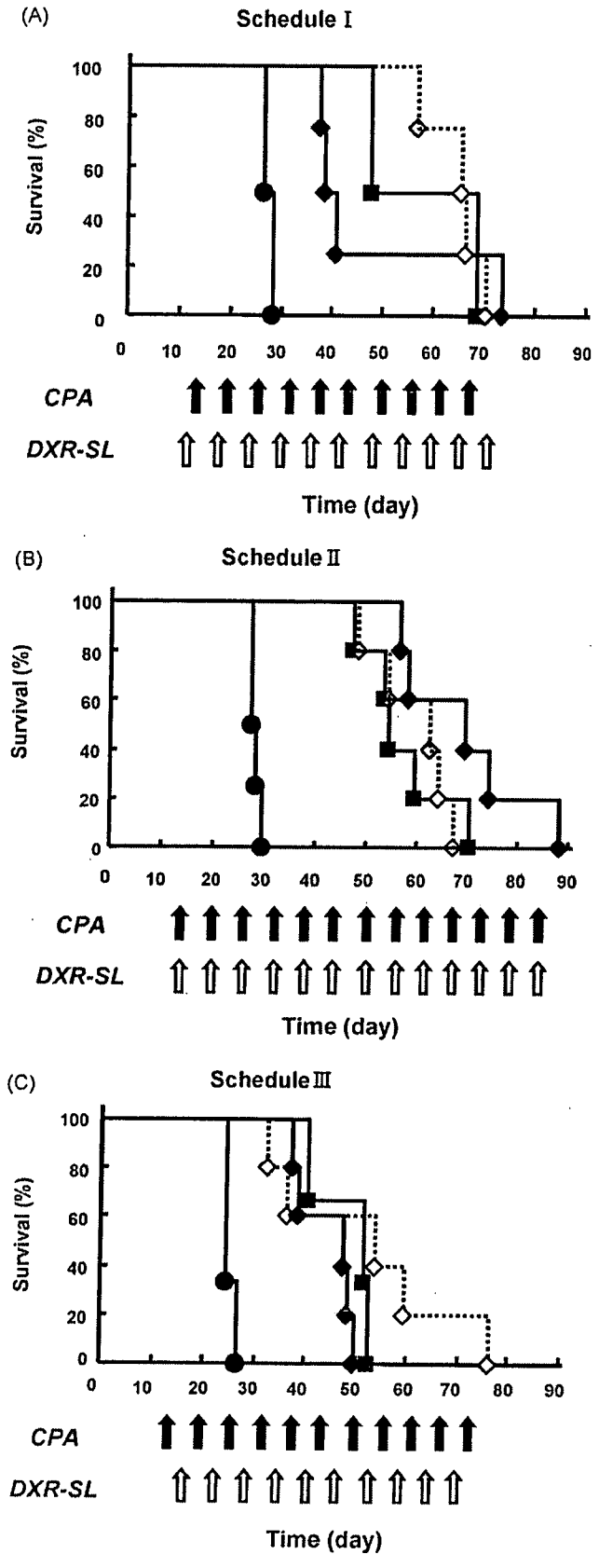

Fig. 3. Effect of the combination of metronomic CPA- and sequential DXR-SL-dosing on survival of B16BL6-bearing mice. (A) Schedule I (low or high dose of DXR-SL): CPA (170 mg/kg) was administered subcutaneously at 6-day intervals. Three days *before* CPA injection (11 days after tumor inoculation), high (5 mg/kg) or low (1 mg/kg) DXR-SL was administered intravenously at 6-day intervals. (B) Schedule II (low or high dose of DXR-SL): CPA (170 mg/kg) was administered subcutaneously and high (5 mg/kg) or low (1 mg/kg) DXR-SL intravenously at 6-day intervals (14 days after tumor inoculation). (C) Schedule III (low or high dose of DXR-SL): CPA (170 mg/kg) was administered subcutaneously at 6-day intervals. Three days *after* the first CPA injection (17 day after tumor inoculation), high (5 mg/kg) or low (1 mg/kg) dose DXR-SL was administered intravenously and the injections were continued at 6-day intervals. Control (●). Metronomic schedule (■), 170 mg/kg administered at 6-day intervals. Combination of metronomic CPA-dosing (170 mg/kg, thin black arrows) and low dose DXR-SL (1 mg/kg, thin gray arrows) (◇ with dotted line). Metronomic CPA-dosing schedule (170 mg/kg, thin black arrows) and high dose DXR-SL (5 mg/kg, thin gray arrows) (◆).

Table 1
Median survival time for each treatment schedule group

	Median survival time (day)			
	None	Schedule I	Schedule II	Schedule III
Control		28.0		
Metronomic dosing		52.0		
CPA (170 mg/kg) + DXR-SL (high, 5 mg/kg)	–	40.5	69.00	51.0
CPA (170 mg/kg) + DXR-SL (low, 1 mg/kg)	–	66.5	63.0	54.0

The results were calculated on the basis of the data presented in Fig. 3.

and III (described in detail in Section 2) were tested in pulmonary metastatic B16BL6 melanoma bearing mice. All MSTs are summarized in Table 1. The combination of a metronomic schedule of CPA with DXR-SL prolonged MST compared to control (non-treatment) (Fig. 3). For Schedule I, only the combination of CPA with the *high* dose of DXR-SL prolonged MST compared with the metronomic schedule of CPA (Fig. 3A, Table 1). In contrast, for Schedule II, the combination of CPA with either the *low* or *high* dose of DXR-SL prolonged MST compared with the metronomic CPA-dosing schedule (Fig. 3B, Table 1). Interestingly, for Schedule III, the combination of CPA with DXR-SL did not prolong, but rather shortened, MST compared with the metronomic CPA-dosing schedule (Fig. 3C, Table 1). The results shown in Fig. 4 indicate that the combined therapy significantly inhibited the growth cells that had metastasized in the lung compared to control (no-treatment). The Schedule I combined therapy significantly inhibited growth of metastasized cells, compared with the metronomic CPA-dosing schedule, regardless of the dose of DXR-SL (Fig. 4A). The Schedule II combined therapy with the high dose of DXR-SL significantly inhibited growth of metastasized cells, while the low dose of DXR-SL did not (Fig. 4B). The Schedule III combined therapy did not induce any significant inhibition of metastatic cell growth (Fig. 4C).

3.4. Toxicity of the combination of the metronomic CPA-dosing schedule and sequential administration of DXR-SL

Because the presence of a tumor influences bone marrow function and because treatment of tumor-bearing mice with chemotherapeutic agents makes data interpretation extremely

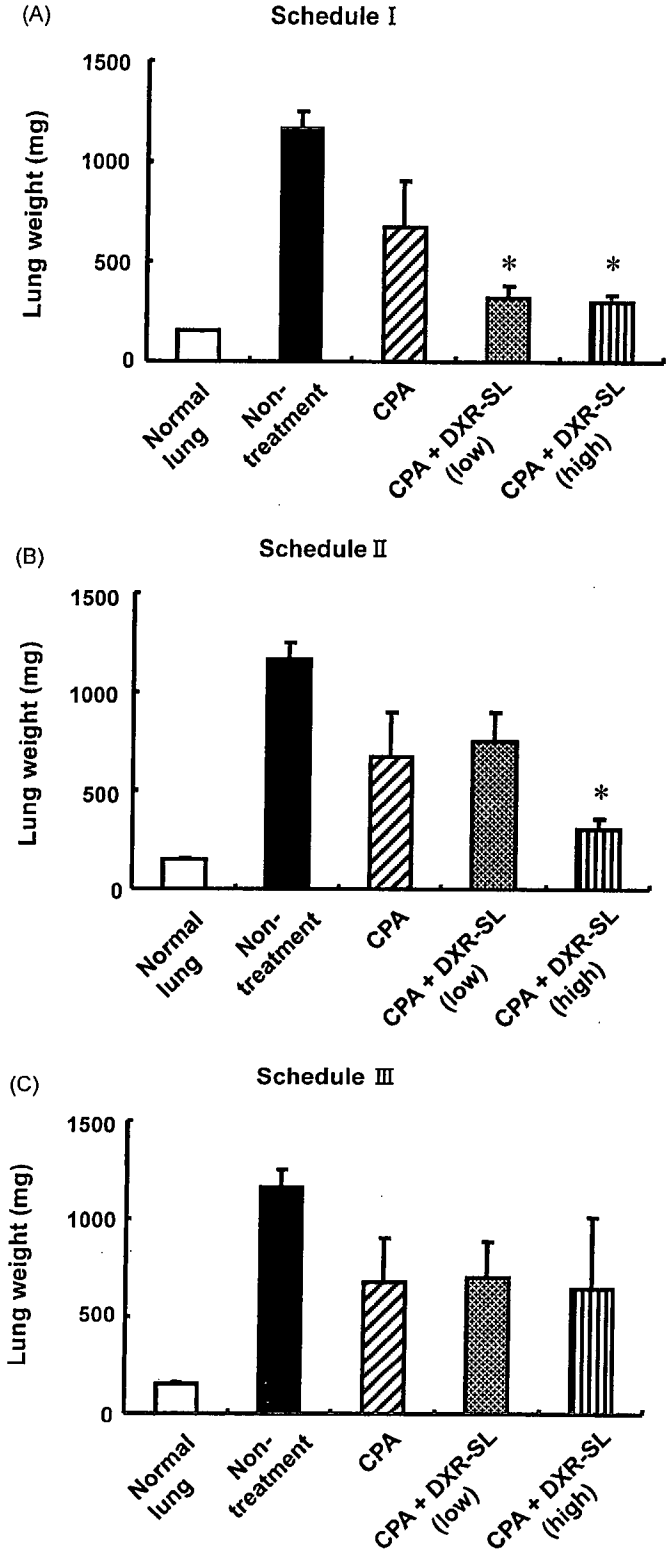

Fig. 4. Effect of the combination of metronomic CPA- and sequential DXR-SL-dosing on lung weight in B16BL6-bearing mice. The dosing schedules used were the same as those described in the legend of Fig. 3: (A) Schedule I (low or high dose of DXR-SL); (B) Schedule II (low or high dose of DXR-SL); (C) Schedule III (low or high dose of DXR-SL). $*p < 0.001$ vs. metronomic CPA-dosing schedule.

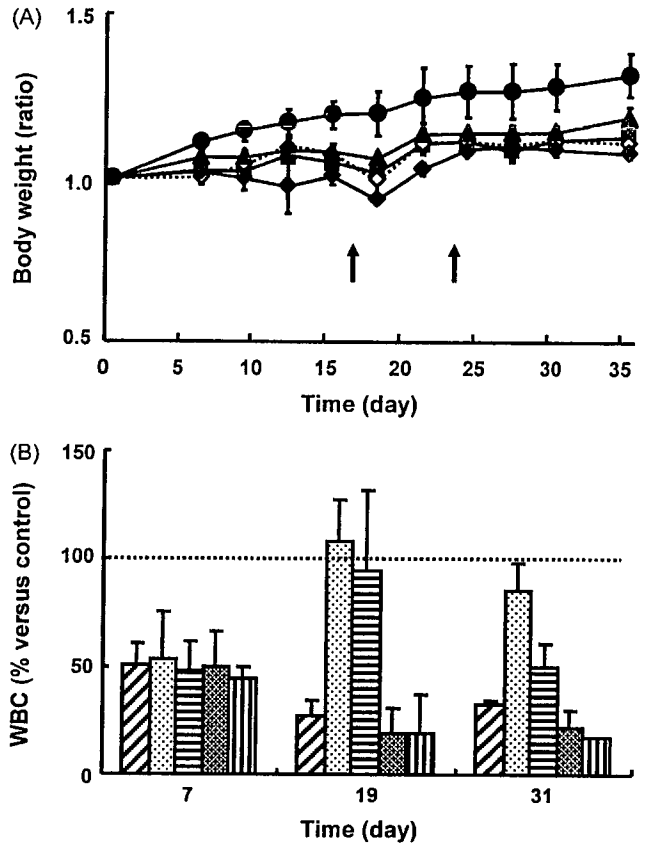

Fig. 5. Toxicity studies for the combination metronomic CPA-dosing plus intravenous administration of DXR-SL. (A) Body weight change. The body weight change expressed as ratio of post-treatment to initial body weight. Control (●), no treatment. CPA (■), 170 mg/kg administered at 6-day intervals. Combination of CPA (170 mg/kg) and low dose DXR-SL (1 mg/kg) administered at 6-day intervals (◊ with dotted line). Combination of CPA (170 mg/kg) and high dose DXR-SL (5 mg/kg) administered at 6-day intervals (♦). DXR-SL (▲), 5 mg/kg administered at 6-day intervals. Arrows indicate time of death for mice treated with combination of CPA (170 mg/kg) and DXR-SL (5 mg/kg). (B) Change in white blood cell number relative to control (no treatment). CPA (▨), 170 mg/kg administered at 6-day intervals. Low dose DXR-SL (▨), 1 mg/kg administered at 6-day intevals. High dose DXR-SL (▤), 5 mg/kg administered at 6-day intervals. Combination of CPA (170 mg/kg) and low dose DXR-SL (1 mg/kg) (▨) administered at 6-day intervals. Combination of CPA (170 mg/kg) and high dose DXR-SL (5 mg/kg) (▤) administered at 6-day intervals.

difficult, the toxicity of the combination therapy of CPA and DXR-SL was examined in not-tumor-bearing mice. In addition, six cycles of the Schedule II combination treatment were employed in the toxicity assessment. At day 35 after initiation of the dosing schedule, the toxicity of the combination therapy was estimated by measuring changes in body weight and WBC number, surrogate markers for treatment-related toxicity.

All combination regimens led to transient weight loss related to growth suppression in treated versus untreated mice (Fig. 5A). Two of the five mice treated with CPA (170 mg/kg) plus the high DXR-SL dose (5 mg/kg) died—one on day 17 and the other on day 24 (Fig. 5A, arrow). This demonstrates that the higher dose of DXR (5 mg/kg) in SL is toxic when combined with CPA. However, tissue weights of treated mice (heart, lung, liver, kidney and spleen) that survived were not different than those of control mice (data not shown).

The metronomic CPA-dosing schedule reduced the number of peripheral WBC (Fig. 5B). DXR-SL also dramatically reduced WBC number, regardless of DXR dose, followed by a rebound in WBC number. The combination regimen (CPA and DXR-SL) reduced the number of WBC, but there was no subsequent rebound in WBC number. The reduction in WBC number with the combination therapy was similar to that observed for the metronomic CPA-dosing schedule. This finding indicates that adding DXR-SL to the metronomic CPA-dosing schedule does not increase the bone marrow toxicity of CPA.

4. Discussion

Metronomic chemotherapy – the frequent administration of an anticancer agent at relatively low, minimally toxic doses with no prolonged drug-free breaks – is a novel approach to the control of advanced cancer. In this study, it was confirmed that the metronomic CPA-dosing schedule exhibited superior therapeutic efficacy in B16BL6-bearing mice, compared with the conventional dosing schedule using the CPA maximum tolerated dose (Fig. 1). Furthermore, the combination of the metronomic CPA-dosing schedule with sequential injections of DXR-SL increased therapeutic efficacy compared to administration of either treatment alone, although the effect was dependent on the schedule and dose of DXR-SL (Figs. 1–3).

Metronomic chemotherapy using CPA is believed to induce apoptosis in the endothelial cells of the growing tumor vasculature (Browder et al., 2000; Kerbel and Kamen, 2004). Thus, it was hypothesized that the metronomic CPA-dosing schedule would increase the permeability of tumor microvessels to macromolecules, including SL, resulting in enhanced accumulation of SL in tumors. Consequently, the therapeutic efficacy of anticancer agents would be enhanced. As expected, the results of the present study showed that some of the combined CPA and DXR-SL dosing schedule had improved therapeutic efficacy (Fig. 3). It should be noted that injection of DXR-SL alone (every 6 days, three times) showed no improvement in MST, regardless of the dose of DXR. Only the high dose of DXR-SL slightly suppressed the growth of cells that had metastasized to the lung (Fig. 2). This result strongly supports the hypothesis that metronomic CPA therapy changes the tumor neovasculature, resulting in enhanced extravasation and subsequent accumulation of SL in tumors. However, the ability of metronomic chemotherapy to enhance the EPR effect remains to be determined.

Interestingly, the improvement was dependent on the dosing schedule, as well as on the DXR-SL dose. Schedule I (low dose of DXR-SL) and Schedule II (high dose of DXR-SL) significantly increased the MST of tumor-bearing mice and inhibited the growth of cells that had metastasized to the lung, compared with the metronomic CPA-dosing schedule (Figs. 3 and 4). In contrast, Schedule III did not increase MST. It is thought that SL, which has a long half-life in circulation, accumulates in solid tumors due to the EPR effect (Jain, 1987; Papahadjopoulos et al., 1991; Wu et al., 1993; Yuan et al., 1995; Forssen et al., 1996; Vaage et al., 1997; Maeda et al., 2000), if the tumor vessels are still permeable. Preclinical and clinical evidence shows that anti-angiogenic therapies normalize the endothelial cells of tumor vessels and consequently decrease vessel permeability (Huber et al., 2005; Jain et al., 2007). These reports describing the biodistribution of SL led to the hypothesis that the metronomic CPA-dosing schedule (an anti-angiogenic therapy) transiently increases tumor vessel permeability and then decreases it as vessels are "normalized". Therefore. It is possible that for Schedule III, according to which DXR-SL is administered 3 days after the first CPA injection, SL accumulation was inhibited, thereby preventing a therapeutic effect (Figs. 3 and 4).

Schedule I (high dose of DXR-SL) resulted in significantly reduced lung weights without any improvement in MST. This apparent inconsistency may be due to enhanced toxicity of the combination of metronomic CPA therapy and intravenous liposomal DXR treatment. Increased toxicity of the combination treatment was supported by the death of two out of five normal mice during six cycles of the combination of CPA and DXR-SL administered at 6-day intervals (Fig. 5A). Furthermore, the combined therapies suppressed weight gain in normal mice. However, it appears that the increased toxicity in this study was not caused by enhancement of the myelosuppressive effects of CPA (Gale, 1985) by the DXR-SL injections (Fig. 5B). Although SL has a long half-life in circulation because of reduced opsonization by serum proteins and lowered recognition by cells of the MPS (Lasic et al., 1991; Torchilin et al., 1994), a fraction of administered SL is ultimately cleared by hepatic macrophages. Daemen et al. (1995, 1997) reported that injection of DXR-SL has a toxic effect on hepatic macrophages, reducing both specific phagocytic activity and cell numbers. Hence, it may be presumed that the toxic effects of CPA and DXR-SL can be either additive or synergistic, resulting in death in some experimental animals.

Other researchers have already demonstrated that the combination of several drugs administered by metronomic dosing with specific antiangiogenic reagents significantly increased the antitumor effects of metronomic dosing (Browder et al., 2000; Klement et al., 2000, 2002; Takahashi et al., 2001; Bello et al., 2001). Recently, Kano et al. (2007) reported that a low dose of transforming growth factor type I receptor (TβR-I) inhibitor promoted accumulation of macromolecules, including nanocarriers (polymeric micelles incorporating DXR), in tumors. TβR-I inhibitor specifically increases the permeability of the tumor neovasculature by decreasing coverage of the endothelium without decreasing endothelial area. This observation clearly suggests that the low dose of TβR-I inhibitor enhances the EPR effect in solid tumors, thereby increasing the therapeutic efficacy of DXR-containing nanocarrier. To the best of our knowledge, this is the first study to demonstrate that the combination of metronomic chemotherapy and liposomal anticancer drug (DXR) treatment increases antitumor effect, presumably by enhancing accumulation of liposomal anti-cancer drugs within the tumor. Thus, the combination of metronomic chemotherapy and liposomal anticancer agents such as Doxil is an innovative strategy in cancer chemotherapy. However, additional studies are needed to determine optimal dosages and treatment schedules to enhance therapeutic efficacy without any adverse effects.

Acknowledgements

We thank Dr. James L. McDonald for his helpful advice in writing the English manuscript. This study was supported by the Kobayashi Fund for Cancer Research and the Knowledge Cluster Initiative from Ministry of Education, Science and Technology.

References

Bartlett, G.R., 1959. Colorimetric assay methods for free and phosphorylated glyceric acids. J. Biol. Chem. 234, 469–471.

Bello, L., Carrabba, G., Giussani, C., Lucini, V., Cerutti, F., Scaglione, F., Landre, J., Pluderi, M., Tomei, G., Villani, R., Carroll, R.S., Black, P.M., Bikfalvi, A., 2001. Low-dose chemotherapy combined with an antiangiogenic drug reduces human glioma growth in vivo. Cancer Res. 61, 7501–7506.

Bolotin, E.M., Cohen, R., Bar, L.K., Emanuel, S.N., Lasic, D.D., Barenholz, Y., 1994. Ammonium sulphate gradients for efficient and stable remote loading of amphipathic weak bases into liposomes and ligandosomes. J. Liposome Res. 4, 455–479.

Browder, T., Butterfield, C.E., Kraling, B.M., Shi, B., Marshall, B., O'Reilly, M.S., Folkman, J., 2000. Antiangiogenic scheduling of chemotherapy improves efficacy against experimental drug-resistant cancer. Cancer Res. 60, 1878–1886.

Daemen, T., Hofstede, G., Ten Kate, M.T., Bakker-Woudenberg, I.A., Scherphof, G.L., 1995. Liposomal doxorubicin-induced toxicity: depletion and impairment of phagocytic activity of liver macrophages. Int. J. Cancer 61, 716–721.

Daemen, T., Regts, J., Meesters, M., Ten Kate, M.T., Bakker-Woudenberg, I.A., Scherphof, G.L., 1997. Toxicity of doxorubicin entrapped within long-circulating liposomes. J. Control. Release 44, 1–9.

Dawson, D.W., Pearce, S.F., Zhong, R., Silverstein, R.L., Frazier, W.A., Bouck, N.P., 1997. CD36 mediates the In vitro inhibitory effects of thrombospondin-1 on endothelial cells. J. Cell Biol. 138, 707–717.

de Fraipont, F., Nicholson, A.C., Feige, J.J., Van Meir, E.G., 2001. Thrombospondins and tumor angiogenesis. Trends Mol. Med. 7, 401–407.

Forssen, E.A., Male-Brune, R., Adler-Moore, J.P., Lee, M.J., Schmidt, P.G., Krasieva, T.B., Shimizu, S., Tromberg, B.J., 1996. Fluorescence imaging studies for the disposition of daunorubicin liposomes (DaunoXome) within tumor tissue. Cancer Res. 56, 2066–2075.

Gale, R.P., 1985. Antineoplastic chemotherapy myelosuppression: mechanisms and new approaches. Exp. Hematol. 13 (Suppl. 16), 3–7.

Gille, J., Spieth, K., Kaufmann, R., 2005. Metronomic low-dose chemotherapy as antiangiogenic therapeutic strategy for cancer. J. Dtsch Dermatol Ges. 3, 26–32.

Grunaug, M., Bogner, J.R., Loch, O., Goebel, F.D., 1998. Liposomal doxorubicin in pulmonary Kaposi's sarcoma: improved survival as compared to patients without liposomal doxorubicin. Eur. J. Med. Res. 3, 13–19.

Guo, N., Krutzsch, H.C., Inman, J.K., Roberts, D.D., 1997. Thrombospondin 1 and type I repeat peptides of thrombospondin 1 specifically induce apoptosis of endothelial cells. Cancer Res. 57, 1735–1742.

Hamano, Y., Sugimoto, H., Soubasakos, M.A., Kieran, M., Olsen, B.R., Lawler, J., Sudhakar, A., Kalluri, R., 2004. Thrombospondin-1 associated with tumor microenvironment contributes to low-dose cyclophosphamide-mediated endothelial cell apoptosis and tumor growth suppression. Cancer Res. 64, 1570–1574.

Huber, P.E., Bischof, M., Jenne, J., Heiland, S., Peschke, P., Saffrich, R., Grone, H.J., Debus, J., Lipson, K.E., Abdollahi, A., 2005. Trimodal cancer treatment: beneficial effects of combined antiangiogenesis, radiation, and chemotherapy. Cancer Res. 65, 3643–3655.

Ishida, T., Maeda, R., Ichihara, M., Irimura, K., Kiwada, H., 2003. Accelerated clearance of PEGylated liposomes in rats after repeated injections. J. Control Release 88, 35–42.

Jain, R.K., 1987. Transport of molecules across tumor vasculature. Cancer Metastasis Rev. 6, 559–593.

Jain, R.K., Tong, R.T., Munn, L.L., 2007. Effect of vascular normalization by antiangiogenic therapy on interstitial hypertension, peritumor edema, and lymphatic metastasis: insights from a mathematical model. Cancer Res. 67, 2729–2735.

Jimenez, B., Volpert, O.V., Crawford, S.E., Febbraio, M., Silverstein, R.L., Bouck, N., 2000. Signals leading to apoptosis-dependent inhibition of neovascularization by thrombospondin-1. Nat. Med. 6, 41–48.

Kano, M.R., Bae, Y., Iwata, C., Morishita, Y., Yashiro, M., Oka, M., Fujii, T., Komuro, A., Kiyono, K., Kaminishi, M., Hirakawa, K., Ouchi, Y., Nishiyama, N., Kataoka, K., Miyazono, K., 2007. Improvement of cancer-targeting therapy, using nanocarriers for intractable solid tumors by inhibition of TGF-beta signaling. Proc. Natl. Acad. Sci. U.S.A. 104, 3460–3465.

Kerbel, R.S., Kamen, B.A., 2004. The anti-angiogenic basis of metronomic chemotherapy. Nat. Rev. Cancer 4, 423–436.

Klement, G., Baruchel, S., Rak, J., Man, S., Clark, K., Hicklin, D.J., Bohlen, P., Kerbel, R.S., 2000. Continuous low-dose therapy with vinblastine and VEGF receptor-2 antibody induces sustained tumor regression without overt toxicity. J. Clin. Invest. 105, R15–R24.

Klement, G., Huang, P., Mayer, B., Green, S.K., Man, S., Bohlen, P., Hicklin, D., Kerbel, R.S., 2002. Differences in therapeutic indexes of combination metronomic chemotherapy and an anti-VEGFR-2 antibody in multidrug-resistant human breast cancer xenografts. Clin. Cancer Res. 8, 221–232.

Klink, T., Bela, C., Stoelting, S., Peters, S.O., Broll, R., Wagner, T., 2006. Metronomic trofosfamide inhibits progression of human lung cancer xenografts by exerting anti-angiogenic effects. J. Cancer Res. Clin. Oncol. 132, 643–652.

Krown, S.E., Northfelt, D.W., Osoba, D., Stewart, J.S., 2004. Use of liposomal anthracyclines in Kaposi's sarcoma. Semin. Oncol. 31, 36–52.

Laquente, B., Vinals, F., Germa, J.R., 2007. Metronomic chemotherapy: an antiangiogenic scheduling. Clin. Transl. Oncol. 9, 93–98.

Lasic, D.D., Martin, F.J., Gabizon, A., Huang, S.K., Papahadjopoulos, D., 1991. Sterically stabilized liposomes: a hypothesis on the molecular origin of the extended circulation times. Biochim. Biophys. Acta 1070, 187–192.

Lawler, J., 2002. Thrombospondin-1 as an endogenous inhibitor of angiogenesis and tumor growth. J. Cell Mol. Med. 6, 1–12.

Li, W., Ishida, T., Okada, Y., Oku, N., Kiwada, H., 2005. Increased gene expression by cationic liposomes (TFL-3) in lung metastases following intravenous injection. Biol. Pharm. Bull. 28, 701–706.

Maeda, H., Wu, J., Sawa, T., Matsumura, Y., Hori, K., 2000. Tumor vascular permeability and the EPR effect in macromolecular therapeutics: a review. J. Control Release 65, 271–284.

Munoz, R., Man, S., Shaked, Y., Lee, C.R., Wong, J., Francia, G., Kerbel, R.S., 2006. Highly efficacious nontoxic preclinical treatment for advanced metastatic breast cancer using combination oral UFT-cyclophosphamide metronomic chemotherapy. Cancer Res. 66, 3386–3391.

Munoz, R., Shaked, Y., Bertolini, F., Emmenegger, U., Man, S., Kerbel, R.S., 2005. Anti-angiogenic treatment of breast cancer using metronomic low-dose chemotherapy. Breast 14, 466–479.

Papahadjopoulos, D., Allen, T.M., Gabizon, A., Mayhew, E., Matthay, K., Huang, S.K., Lee, K.D., Woodle, M.C., Lasic, D.D., Redemann, C., Martin, F.J., 1991. Sterically stabilized liposomes: improvements in pharmacokinetics and antitumor therapeutic efficacy. Proc. Natl. Acad. Sci. U.S.A. 88, 11460–11464.

Safra, T., Muggia, F., Jeffers, S., Tsao-Wei, D.D., Groshen, S., Lyass, O., Henderson, R., Berry, G., Gabizon, A., 2000. Pegylated liposomal doxorubicin (doxil): reduced clinical cardiotoxicity in patients reaching or exceeding cumulative doses of 500 mg/m^2. Ann. Oncol. 11, 1029–1033.

Shaked, Y., Emmenegger, U., Man, S., Cervi, D., Bertolini, F., Ben-David, Y., Kerbel, R.S., 2005. Optimal biologic dose of metronomic chemotherapy regimens is associated with maximum antiangiogenic activity. Blood 106, 3058–3061.

Takahashi, N., Haba, A., Matsuno, F., Seon, B.K., 2001. Antiangiogenic therapy of established tumors in human skin/severe combined immunodeficiency mouse chimeras by anti-endoglin (CD105) monoclonal antibodies, and synergy between anti-endoglin antibody and cyclophosphamide. Cancer Res. 61, 7846–7854.

Tonini, G., Schiavon, G., Silletta, M., Vincenzi, B., Santini, D., 2007. Antiangiogenic properties of metronomic chemotherapy in breast cancer. Future Oncol. 3, 183–190.

Torchilin, V.P., Omelyanenko, V.G., Papisov, M.I., Bogdanov Jr., A.A., Trubetskoy, V.S., Herron, J.N., Gentry, C.A., 1994. Poly(ethylene glycol) on the liposome surface: on the mechanism of polymer-coated liposome longevity. Biochim. Biophys. Acta 1195, 11–20.

Vaage, J., Donovan, D., Uster, P., Working, P., 1997. Tumour uptake of doxorubicin in polyethylene glycol-coated liposomes and therapeutic effect against a xenografted human pancreatic carcinoma. Br. J. Cancer 75, 482–486.

Wu, N.Z., Da, D., Rudoll, T.L., Needham, D., Whorton, A.R., Dewhirst, M.W., 1993. Increased microvascular permeability contributes to preferential accumulation of Stealth liposomes in tumor tissue. Cancer Res. 53, 3765–3770.

Yuan, F., Dellian, M., Fukumura, D., Leunig, M., Berk, D.A., Torchilin, V.P., Jain, R.K., 1995. Vascular permeability in a human tumor xenograft: molecular size dependence and cutoff size. Cancer Res. 55, 3752–3756.

Available online at www.sciencedirect.com
ScienceDirect
International Journal of Pharmaceutics 342 (2007) 194–200
INTERNATIONAL JOURNAL OF PHARMACEUTICS
www.elsevier.com/locate/ijpharm

Pharmaceutical Nanotechnology

Tumor targeting of doxorubicin by anti-MT1-MMP antibody-modified PEG liposomes

Hiroto Hatakeyama [a], Hidetaka Akita [a], Emi Ishida [b], Koichi Hashimoto [b], Hideo Kobayashi [b], Takanori Aoki [c], Junko Yasuda [c], Kenichi Obata [c], Hiroshi Kikuchi [b], Tatsuhiro Ishida [d], Hiroshi Kiwada [d], Hideyoshi Harashima [a,*]

[a] *Graduate School of Pharmaceutical Sciences, Hokkaido University, Sapporo, Hokkaido 060-0812, Japan*
[b] *Daiichi Pharmaceutical Co. Ltd., Tokyo 134-8630, Japan*
[c] *Daiichi Fine Chemical Co. Ltd., Takaoka, Toyama 933-8511, Japan*
[d] *Faculty of Pharmaceutical Sciences, The University of Tokushima, Tokushima 770-8505, Japan*

Received 27 October 2006; received in revised form 23 March 2007; accepted 24 April 2007
Available online 10 May 2007

Abstract

Immunoliposomes are potent carriers for targeting of therapeutic drugs to specific cells. Membrane type-1 matrix metalloproteinase (MT1-MMP), which plays an important role in angiogenesis, is expressed on angiogenic endothelium cells as well as tumor cells. Then, the MT1-MMP might be useful as a target molecule for tumor and neovascularity. In the present study, we addressed a utility of antibodies against the MT1-MMP as a targeting ligand of liposomal anticancer drug. Fab′ fragments of antibody against the MT1-MMP were modified at distal end of polyethylene glycol (PEG) of doxorubicin (DXR)-encapsulating liposomes, DXR-sterically stabilized immunoliposomes (DXR-SIL[anti-MT1-MMP(Fab′)]). Modification with the antibody significantly enhanced cellular uptake of DXR-SIL[anti-MT1-MMP(Fab′)] into the HT1080 cells, which highly express MT1-MMP, compared with the non-targeted liposomes (DXR-stealthliposomes (DXR-SL)), suggesting that MT1-MMP antibody (Fab′) is a potent targeting ligand for the MT1-MMP expressed cells. *In vivo* systemic administration of DXR-SIL[anti-MT1-MMP(Fab′)] into the tumor-bearing mice showed significant suppression of tumor growth compared to DXR-SL. This is presumably due to the active targeting of immunoliposomes for tumor and neovascularity. However, tumor accumulation of DXR-SIL[anti-MT1-MMP(Fab′)] and DXR-SL were comparable, suggesting that both liposomal formulations accumulated in tumor via enhanced permeation and retention (EPR) effect, but not via targeting to the MT1-MMP expressed on both the endothelial and tumor cells. It appears that the enhanced antitumor activity of DXR-SIL[anti-MT1-MMP(Fab′)] resulted from acceleration of cellular uptake of lioposomes owing to the incorporated antibody after extravasation from capillaries in tumor.

Keywords: Immunoliposomes; Cancer therapy; Drug delivery; Matrix metalloproteinase

1. Introduction

Sterically stabilized polyethyleneglycol (PEG)-modified liposomes have already been optimized for escaping uptake by reticuloendothelial system (RES) and prolonging systemic circulation (Klibanov et al., 1990), which resulted in increased accumulation in tumor tissue by enhanced permeation and retention (EPR) effect (Matsumura and Maeda, 1986). Notably, PEGylated liposomes encapsulating doxorubicin (Doxil®) are currently used in clinics. Targeting of liposomes to specific cells is a promising strategy for reducing side effects and improving therapeutic effects. To date, immunoliposomes, in which antibodies were conjugated at the distal end of PEG, were used as carriers. For example, antibodies against vascular cell adhesion molecule-1 (VCAM-1) (Voinea et al., 2005) and insulin receptor (Zhang et al., 2003) for inflammatory tissue and brain, respectively, and epidermal growth factor receptor (EGFR) (Mendelsohnand and Baselga, 2003), transferrin receptors (TfR) (Pardridge, 2004; Xu et al., 2002) were utilized as targets for the cancer cells. Furthermore, the modification of Doxil® with antinuclear autoantibodies against nucleosomes possesses an ability

* Corresponding author at: Faculty of Pharmaceutical Sciences, Hokkaido University, Sapporo, Hokkaido 060-0812, Japan. Tel.: +81 11 706 3919; fax: +81 11 706 4879.
E-mail address: harasima@pharm.hokudai.ac.jp (H. Harashima).

0378-5173/$ – see front matter © 2007 Elsevier B.V. All rights reserved.
doi:10.1016/j.ijpharm.2007.04.037

to specifically recognize the surface of numerous tumor cells, but not normal cells (Lukyanov et al., 2004). Generally, immunoliposomes modified with Fab′ fragment exhibit longer systemic circulation compared with that modified with whole IgG since RES uptakes immunoliposomes via the Fc receptor-mediated mechanism (Maruyama et al., 1997).

Recent progress in cancer physiology revealed that tumor growth is closely related to the development of new blood vessels. Then, inhibition of neovascularity is a potent strategy for cancer therapy. One of the key proteins on angiogenesis in tumor vessels is membrane type-1 matrix metalloproteinase (MT1-MMP), which is expressed on the neovascularity as well as tumor cells. On the plasma membrane, MT1-MMP cleaved extracellular matrix components such as collagen, laminin, fibronectin and elastin (Knauper et al., 1996; Noel et al., 1995; Ohuchi et al., 1997; Pei et al., 1994; Pei and Weiss, 1996; Sato et al., 1994; Strongin et al., 1995). Simultaneously, MT1-MMP activates soluble MMPs (i.e. MMP-2) via its proteolytic activity, which also plays an important role in the degradation of the matrix (Knauper et al., 1996; Ohuchi et al., 1997; Pei and Weiss, 1996; Sato et al., 1994; Strongin et al., 1995). In fact, administration of the inhibitors for MMP families to the tumor-bearing mouse suppressed the angiogenesis, which resulted in the antitumor effect (Maekawa et al., 1999; Nelson, 1998). Based on previous report, dual targeting of antitumor drugs to the neovascular cells and tumor cells are expected to be excellent strategy for the cancer therapy (Maeda et al., 2004). To realize this strategy, we established the doxorubicin-encapsulating sterically stabilized immunoliposome (DXR-SIL[anti-MT1-MMP(Fab′)]), in which Fab′ fragment ($Fab'_{222\text{-}1D8}$) derived from anti-human MT1-MMP monoclonal antibody was modified at the distal end of PEG. In the present study, utility of these immounoliposomes were assessed in both *in vitro* cellular uptake and *in vivo* antitumor effect between DXR-SIL[anti-MT1-MMP(Fab′)] and non-targeted doxorubicin-encapsulating sterically stabilized liposomes (DXR-SL).

2. Methods and materials

2.1. Materials

Cholesterol (CH), distearoyl-*sn*-glycero-3-phoshoethanolamine-*N*-[methoxy(polyethylene glycol)-2000] (DSPE-PEG), hydrogenated soy phosphatidylcholine (HSPC), cysteamine hydrochloride were purchased from WAKO (Osaka, Japan), Genzyme (Cambridge, MS, USA) and Lipoid (Ludwigshafen, Germany). DSPE-PEG with a functional maleimide moiety at the terminal end of PEG: *N*-[(3-maleimide-1-oxopropyl)aminopropyl polyethyleneglycol-carbamyl] distearoylphosphatidyl-ethanolamine (DSPE-PEG-Mal) was purchased from Shearwater (Enschede, The Netherlands). Doxorubicin (DXR) was purchased from Sicor Inc. (Irvine, CA, USA). Ultrogel Ac54 and Sepharose CL-5B were purchased from Pall Biosepra (St. Christophe, France) and Amersham Pharmacia (Arlington Heights, IL, USA). *N*-Ethylmaleimide was purchased from Nacalai Tesque (Kyoto, Japan).

2.2. Animal and cell line

Male BALB/c nude mice (5–6 weeks old) were purchased from CLEA Japan (Tokyo, Japan). All *in vivo* experiments were approved by the Institutional Animal Care and Use Committee. HT1080 cells were purchased from RIKEN Cell Bank and cultured in DMEM supplemented with 10% fetal bovine serum (FBS), penicillin (100 U/ml), streptomycin (100 μg/ml) at 37 °C with 5% CO_2 and 95% humidity on the bottom of a dish (Corning).

2.3. Preparation of Fab′ fragment

Fab′ fragment was prepared from anti-MT1-MMP monoclonal antibody (222-1D8) (Aoki et al., 2002). A volume of 1 ml of the IgG (10 mg/ml) was dialyzed against 0.1 M sodium acetate buffer (pH4.2) containing 0.1 M NaCl, and then added with pepsin at a concentration of 2% (w/w) based on the amount of antibodies and digested at 37 °C. After the incubation for 20 h, the digested product was added with 0.2 ml of 3 M Tris–HCl (pH7.5) to terminate the reaction. The whole digestion product was loaded on an Ultrogel AcA54 gel filtration column (diameter 1.5 cm × length 47 cm) equilibrated with 0.1 M phosphate buffer (pH 7.0) and collected as 1 ml fractions. Elution of $F(ab')_2$ was monitored by UV adsorption (A280). The resulting $F(ab')_2$ was adjusted to a volume of 0.9 ml with 0.1 M phosphate buffer (pH 6.0), supplied with 0.1 ml of 0.1 M cysteamine hydrochloride (final concentration: 0.01 M) and thereby reduced at 37 °C for 1.5 h. The resultant was loaded on an Ultrogel AcA54 gel filtration column (diameter 1.5 cm × length 47 cm) equilibrated with PBS containing 5 mM EDTA and collected as 1 ml fractions. The elution of Fab′ was monitored by A280.

2.4. Preparation of immunoliposomes (DXR-SIL[anti-MT1-MMP(Fab′)])

Lipid film composed of 47.4 mM HSPC/CH (6:4 molar ratio) was prepared by the evaporation. The lipid film was hydrated with 155 mM ammonium sulfate at pH 5.5, and then particle size of liposomes was controlled by sequential extrusion through polycarbonate membrane filter of 0.2, 0.1, 0.05 μm pore diameter. The extruded liposomes were centrifuged at 300,000 × *g* for 1 h at 4 °C and then resuspended in saline. DXR or [^{14}C]-labeled DXR ([^{14}C]-DXR) was incubated with actively loaded into the liposomes following an ammonium sulfate gradient as described previously (Haran et al., 1993). Then, liposomes were PEGylated by incubating with 0.25 mM of DSPE-PEG or DSPE-PEG/DSPE-PEG-Mal (9:1 molar ratio) for 15 min at 65 °C. Sterically stabilized liposomes (DXR-SL) were centrifuged at 300,000 × *g* for 1 h at 4 °C to remove unloaded DXR and then resuspended in saline to remove unloaded DXR.

To conjugate the Fab′ fragment (1.96 mg/0.37 ml), 0.41 ml of maleimide-introduced liposomes (maleimide concentration: 104 nmol/ml) were mixed with Fab′ fragment (the molar ratio of maleimide moiety and Fab′ fraction was 3:1). After the incubation for 20 h at 4 °C under light shielding, unreacted mercapto groups were blocked by adding 4.3 μl of 0.1 M *N*-

ethylmaleimide. To remove free Fab′ fragment, the reaction mixture was loaded on an Sepharose CL-4B gel filtration column (diameter 3 cm × length 50 cm) equilibrated with PBS and collected as 2 ml fractions. The concentration of cholesterol was quantified by cholesterol *E*-test WAKO kit (Wako: Osaka, Japan). The particle size of liposomes was determined by dynamic light scattering (DLS) (ELS-8000, Otsuka Electronics, Japan).

2.5. In vitro cellular uptake study

To visually compare the cellular uptake of DXR-SIL[anti-MT1-MMP(Fab′)] and DXR-SIL, 5×10^4 cells/dish of HT1080 cells were plated into 3.5 cm dish. DXR-SL or DXR-SIL[anti-MT1-MMP(Fab′)] (14.5 μM of total lipid) were applied and incubated for 3 h at 37 °C, and then washed by Krebs-Henseleit buffer (118 mM NaCl, 23.8 mM $NaHCO_3$, 4.83 mM KCl, 0.96 mM KH_2PO_4, 1.20 mM $MgSO_4$, 12.5 mM HEPES, 5 mM glucose, and 1.53 mM $CaCl_2$ adjusted to pH 7.4). Images were collected by confocal laser scanning microscopy (CLSM) (LSM510 META, Carl Zeiss, Germany). For the quantitative cellular uptake analysis, cells were seeded in 12-well plates at a density of 4×10^4 cells/well 24 h before the transport assay. All transport assays were performed in Krebs-Henseleit buffer. The cells were washed by Krebs-Henseleit buffer. The [^{14}C]-DXR-SIL[anti-MT1-MMP(Fab′)] and [^{14}C]-DXR-SL were added to the Krebs-Henseleit buffer (14.5 μM of total lipid), followed by incubation for 10 min, 1 h and 3 h at 37 °C. Just before the designated times, 50 μl Krebs-Henseleit buffer was transferred to scintillation vials. Then cells were washed with 2 ml ice-cold Krebs-Henseleit buffer to remove the liposomes binding to cell surface and solubilized in 500 μl 1N NaOH. After adding 250 μl 2N HCl, 500 μl aliquots were transferred to scintillation vials. The radioactivity of the cells and Krebs-Henseleit buffer was determined by liquid scintillation counting (LS 6000SE; Beckman Instruments Inc., Fullerton, CA, USA) after 4.5 ml scintillation fluid (Hionic fluor; Packard Instrument Co., Downers Grove, IL, USA) was added to the scintillation vials. The remaining 100 μl aliquots of cell lysate were used to determine protein concentrations by the BCA protein assay kit (PIERCE, Rockford, IL, USA) with BSA as a standard. The uptake of liposomes is given as the volume of distribution, determined as the amount of ligands associated with the cells normalized by the medium concentration.

2.6. Evaluation of in vivo pharmacological effect

Tumor-bearing mice were prepared by s.c. inoculation of a suspension (1×10^6 cells per 100 μl PBS) of HT1080 into BALB/c nude mice. DXR-SIL[anti-MT1-MMP(Fab′)] and DXR-SL were administered at a dose of 3 mg/kg DXR (corresponding to 5 μmol lipid/mouse) to tumor-bearing mice via the tail vein when tumor size was in the range from 1000 to 3000 mm^3. The tumor size was measured up to 12 days after administration. Data were represented as a relative tumor volume normalized by that when liposomes were injected. The antitumor effect was defined as the percent of tumor volume at the indicated times to that at day 0.

2.7. Comparison of in vivo tumor distribution

[^{14}C]-DXR-SIL[anti-MT1-MMP(Fab′)] and [^{14}C]-DXR-SL at a dose of 0.15 μmol lipid/mouse was injected to tumor-bearing mice from the tail vein at 11 days after tumor implantation. At 48 h post-injection, the mice were sacrificed and blood and tumor tissue were collected. The blood and tumor sample were solubilized in Soluene-350 for 5 h at 50 °C. The solubilized blood sample was decolorized by H_2O_2. The radioactivities were determined by liquid scintillation counter with Hionic Fluor.

3. Results and discussion

3.1. Characterization of immunoliposomes

The average particle size of DXR-SIL[anti-MT1-MMP(Fab′)] and DXR-SL was in the range of 85–90 nm and encapsulated ratio of DXR was >97%. The number of Fab′ fragment attached to the distal end of the PEG was approximately 40 molecules, which was calculated as described previously (Hatakeyama et al., 2004).

3.2. Comparison of in vitro cellular uptake

The cellular uptake of DXR encapsulated in SIL[anti-MT1-MMP(Fab′)] and SL by the MT1-MMP-expressing HT1080 cells was compared (Fig. 1). In CLSM analysis, fluorescence signal of DXR was only a slightly detected in SL, whereas strong fluorescence of DXR was detected in SIL[anti-MT1-MMP(Fab′)] (Fig. 1A). The modification with the antibody accelerated cellular uptake of the liposomes. In the quantitative cellular uptake study, the cellular uptake of the both liposomes was increased in time-dependent manner and was stimulated by the modification with Fab′ by approximately five-fold, as compared with non-targeted liposomes (DXR-SL) (Fig. 1B). Since DXR is hydrophobic, it can efficiently diffuse into the cells. However, it is confirmed that leakage of encapsulated DXR in the medium was negligible (retention efficiency >97%, up to 24 h). Collectively, these data indicated that DXR-SIL[anti-MT1-MMP(Fab′)] is efficiently bound to the MT1-MMP-expressing cells, and then is internalized. Considering that the function of MT1-MMP was regulated by endocytosis and recycling (Itoh and Seiki, 2004; Uekita et al., 2001; Wang et al., 2004), the DXR-SIL[anti-MT1-MMP(Fab′)] was also taken up via receptor-mediated endocytosis.

3.3. Comparison of antitumor effect

DXR-SL shows more efficient anti-cancer effects than free DXR, since free DXR are distributed in various organs in non-specific manner (Čeh et al., 1997). To address the utility of DXR-SIL[anti-MT1-MMP(Fab′)] from the view point of *in vivo* antitumor effect, DXR-SIL[anti-MT1-MMP(Fab′)] and DXR-SL were intravenously administered to the tumor-bearing mice